

Collapse of a molecular cloud core to stellar densities: the formation and evolution of pre-stellar discs

Matthew R. Bate*

*School of Physics, University of Exeter, Stocker Road, Exeter EX4 4QL
Monash Centre for Astrophysics, School of Mathematical Sciences, Monash University, Clayton, Vic 3168, Australia*

22 October 2018

ABSTRACT

We report results from radiation hydrodynamical simulations of the collapse of molecular cloud cores to form protostars. The calculations follow the formation and evolution of the first hydrostatic core/disc, the collapse to form a stellar core, and effect of stellar core formation on the surrounding disc and envelope. Past barotropic calculations have shown that rapidly-rotating first cores evolve into ‘pre-stellar discs’ with radii up to ~ 100 AU that may last thousands of years before a stellar core forms. We investigate how the inclusion of a realistic equation of state and radiative transfer alters this behaviour, finding that the qualitative behaviour is similar, but that the pre-stellar discs may last 1.5 – 3 times longer in the more realistic calculations. The masses, radii, and lifetimes of the discs increase for initial molecular cloud cores with faster rotation rates. In the most extreme case we model, a pre-stellar disc with a mass of $0.22 M_{\odot}$ and a radius of ≈ 100 AU can form in a $1-M_{\odot}$ cloud and last several thousand years before a stellar core is formed. Such large, massive objects may be imaged using ALMA. Fragmentation of these massive discs may also provide an effective route to binary and multiple star formation, before radiative feedback from accretion onto the stellar core can inhibit fragmentation. Once collapse to form a stellar core occurs within the pre-stellar disc, the radiation hydrodynamical simulations produce qualitatively different behaviour from the barotropic calculations due to the accretion energy released. This drives a shock wave through the circumstellar disc and launches a bipolar outflow even in the absence of magnetic fields.

Key words: accretion, accretion discs – hydrodynamics – radiative transfer – stars: formation – stars: low-mass, brown dwarfs – stars: winds, outflows.

1 INTRODUCTION

The first numerical calculations of the collapse of a molecular cloud core to stellar core formation, and beyond, were performed by Larson (1969) more than four decades ago. These one-dimensional radiation hydrodynamical calculations revealed the main stages of protostar formation: an almost isothermal collapse until the inner regions become optically thick, the almost adiabatic formation of the first hydrostatic core (typical radius ≈ 5 AU and initial mass $\approx 5 M_{\text{J}}$), the growth of this core as it accreted from the infalling envelope, the second collapse within this core triggered by the dissociation of molecular hydrogen, the formation of the stellar core (initial radius $\approx 2 R_{\odot}$ and mass $\approx 1.5 M_{\text{J}}$), and, lastly, the long accretion phase of the stellar core to its final mass. More recent one-dimensional studies (e.g. Masunaga & Inutsuka 2000; Commerçon et al. 2011) have not altered this picture.

However, in one-dimension, the effects of rotation and magnetic fields can not be examined. Larson (1972) began per-

forming two-dimensional calculation of rotating clouds soon after his ground-breaking one-dimensional calculations. But multi-dimensional calculations are considerably more time consuming and it was not until almost two decades after the first one-dimensional models that the first two dimensional calculations were able to follow the collapse to the formation of the stellar core (Tscharnuter 1987). These calculations showed that with rotation, both the first hydrostatic core and the later-formed stellar core became rotationally-flattened and allowed the shock structures in the accretion flows to be studied in detail (e.g. Tscharnuter et al. 2009).

It was not until nearly three decades after Larson’s original calculations that the first three-dimensional calculations following the collapse to stellar core formation were possible. Bate (1998) performed three-dimensional calculations of rotating molecular cloud cores using a barotropic equation of state to mimic the effects of a realistic equation of state and radiative transfer. He found that if the original molecular cloud core was rotating rapidly enough, the rotationally-flattened first hydrostatic core could be dynamically unstable to the growth of non-axisymmetric perturbations. It deformed into a bar, followed by the wrapping up of the ends of the

* E-mail: mbate@astro.ex.ac.uk

bar into a disc with strong trailing spiral arms. Gravitational torques removed angular momentum and rotational support from the inner regions of the first core, quickening the onset of the second collapse and inhibiting fragmentation during the second collapse phase. The development of a bar-mode and spiral structure is expected for rapidly-rotating polytropic-like structures (e.g. Durisen et al. 1986). Such instabilities occur when the ratio of the rotational energy to the magnitude of the gravitational potential energy of the first core exceeds $\beta = 0.274$. Bate was also the first to point out that because a rapidly-rotating first core develops into a disc before the stellar core forms, the *disc forms before the star*. Rather than hydrostatic cores, such structures are better described as ‘pre-stellar discs’. Once the second collapse occurred and a stellar core formed, Bate found an inner disc formed around the stellar core and grew in radius as material with larger angular momentum fell in. Bate speculated that if the calculation were able to be followed further, the outer radius of the inner disc would eventually grow to join on to the outer disc, leaving the stellar core surrounded by a single large disc.

The next major advance in this field was to begin including the effects of magnetic fields. Tomisaka (2002) was the first to follow the collapse of a molecular cloud core to stellar densities including magnetic fields. Using two-dimensional calculations, he found that both the first core and stellar cores launched magnetically-driven outflows. This work has been followed by a number of papers using three-dimensional calculations to investigate magnetised collapse and outflows (Machida et al. 2005, 2006, 2008) and the rotation rates and magnetic field strengths in the first and stellar cores (Machida et al. 2007). At the same time, the development of non-axisymmetric structure at the first core stage and the formation of a pre-stellar disc discovered by Bate (1998) and fragmentation has been studied further both without (Saigo & Tomisaka 2006; Saigo et al. 2008; Saigo & Tomisaka 2011) and with magnetic fields (Machida et al. 2005, 2010; Machida & Matsumoto 2011). With the increasing capability of observational instruments and, in particular, looking forward to the capabilities of the Atacama Large Millimeter/submillimeter Array (ALMA), some of these works also began to investigate the observational signatures of the first core phase such as their luminosities (Saigo & Tomisaka 2006), spectral energy distributions (SEDs), and images (Saigo & Tomisaka 2011).

However, all three-dimensional studies listed above have used barotropic equations of state rather than realistic equations of state with radiative transfer. The first three-dimensional calculations including radiative transfer that followed collapse to the point of stellar core formation (but not beyond) were Whitehouse & Bate (2006), using the flux-limited diffusion approximation, and Stamatellos et al. (2007), using a radiative cooling approximation. Bate (2010) investigated the evolution of both first and stellar cores using radiation hydrodynamical calculations. He found that the evolution up until stellar core formation was qualitatively similar to that obtained with a barotropic equation of state, including bar-mode instabilities and stellar core formation. However, following the formation of the stellar core, the energy released has a dramatic effect on the surrounding disc and envelope and launches a temporary outflow even in the absence of a magnetic field. Recent two-dimensional radiation hydrodynamical simulations that follow the collapse to stellar densities and well beyond as the stellar core accretes from the infalling envelope (Schönke & Tscharnuter 2011) show a similar effect, where the formation of the stellar core drives a temporary outflow.

The most complete three-dimensional calculations of the collapse of molecular cloud cores to date include radiation hydrody-

namics and magnetic fields (Tomida et al. 2010a; Tomida et al. 2010b; Commerçon et al. 2011). As with the past magnetised barotropic calculations, the first core is found to launch outflows, but now the thermodynamics of the gas is more properly treated. However, these models only study the evolution of the first core, and do not follow the second collapse and formation of the stellar core.

In this paper, we extend the study of Bate (2010) who presented the first three-dimensional radiation hydrodynamical calculations to follow the collapse beyond the formation of the stellar core. Bate only presented results for one particular value of the rotation rate of the molecular cloud core. Here we investigate how the evolution of the first core or pre-stellar disc varies with different rotation rates, and we compare the results obtained using radiation hydrodynamics with those obtained using a barotropic equation of state. We also study how the thermally-launched outflows following stellar core formation depend on the rotation rate, and how the discs evolve. Finally, we perform many of the calculations at several different numerical resolutions to test the effects of numerical resolution and examine convergence.

2 COMPUTATIONAL METHOD

The calculations presented here were performed using a three-dimensional smoothed particle hydrodynamics (SPH) code based on the original version of Benz (1990; Benz et al. 1990), but substantially modified as described in Bate et al. (1995), Whitehouse, Bate & Monaghan (2005), Whitehouse & Bate (2006), Price & Bate (2007), and parallelised using both OpenMP and MPI.

Gravitational forces between particles and a particle’s nearest neighbours are calculated using a binary tree. The smoothing lengths of particles are variable in time and space, set iteratively such that the smoothing length of each particle $h = 1.2(m/\rho)^{1/3}$ where m and ρ are the SPH particle’s mass and density, respectively (see Price & Monaghan 2007, for further details). The SPH equations are integrated using a second-order Runge-Kutta-Fehlberg integrator with individual time steps for each particle (Bate et al. 1995). To reduce numerical shear viscosity, we use the Morris & Monaghan (1997) artificial viscosity with α_v varying between 0.1 and 1 while $\beta_v = 2\alpha_v$ (see also Price & Monaghan 2005).

2.1 Equation of state and radiative transfer

The calculations presented in this paper, use two different types of equation of state. The first is a barotropic equation of state, almost identical to that used by Bate (1998), where the temperature of the gas depends only on its density. In this case, the thermal pressure of the gas $p = K\rho^\eta$. The value of the effective polytropic exponent η , varies with density as

$$\eta = \begin{cases} 1, & \rho \leq 1.0 \times 10^{-13} \\ 7/5, & 1.0 \times 10^{-13} < \rho \leq 5.7 \times 10^{-8} \\ 1.15, & 5.7 \times 10^{-8} < \rho < 1.0 \times 10^{-3} \\ 5/3, & \rho > 1.0 \times 10^{-3}. \end{cases} \quad (1)$$

We take the mean molecular weight of the gas to be $\mu = 2.38$. The value of K is defined such that when the gas is isothermal $K = c_s^2$, with the sound speed $c_s = 2.04 \times 10^4 \text{ cm s}^{-1}$, and the pressure is continuous when the value of η changes.

The second type of calculation is performed using radiation hydrodynamics. In this case, we use an ideal gas equation of state $p = \rho T \mathcal{R} / \mu$, where T is the gas temperature, and \mathcal{R} is the gas

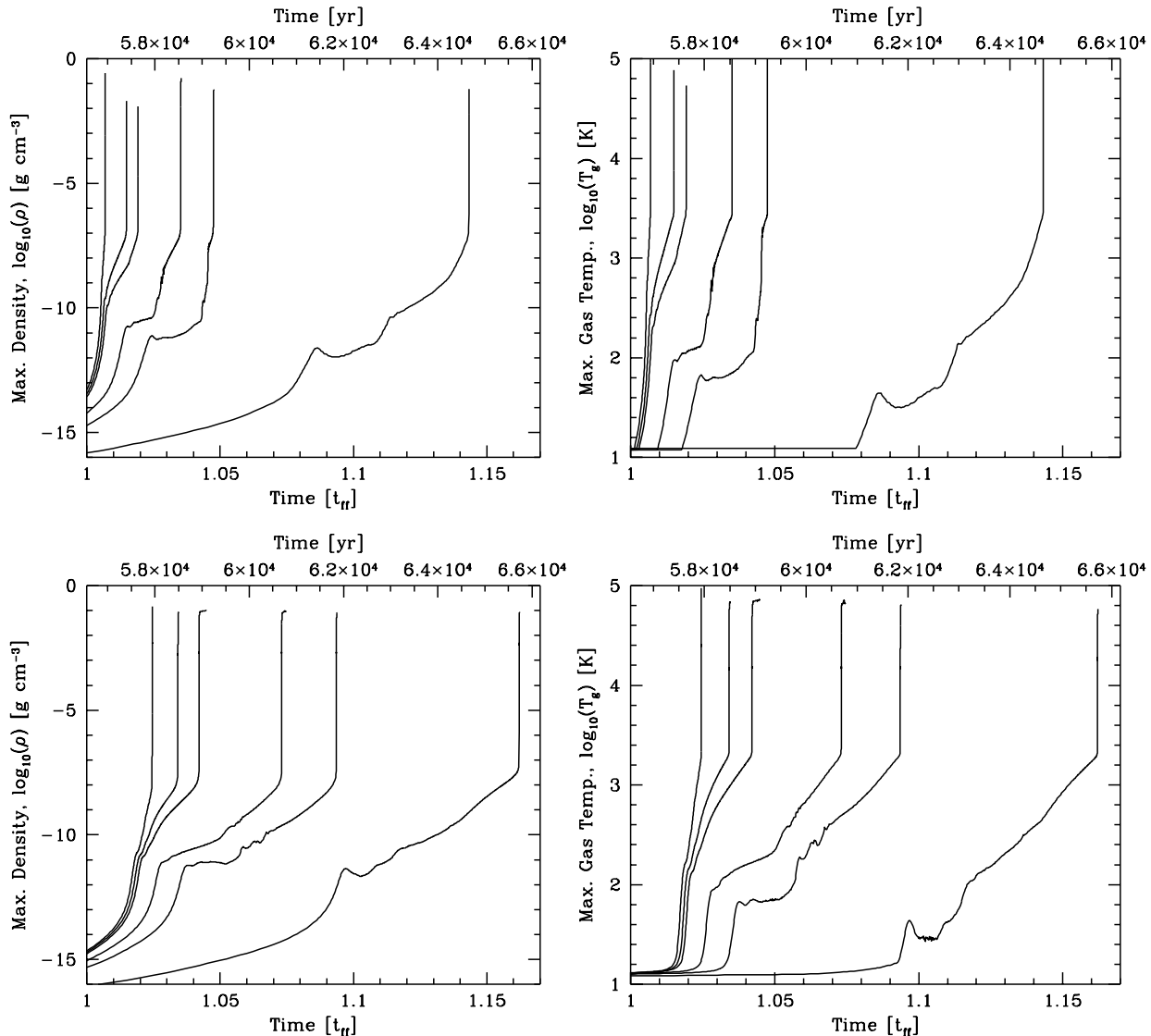


Figure 1. The time evolution of the maximum density (left panels) and gas temperature (right panels) during the barotropic calculations (top panels) and the radiation hydrodynamical calculations (bottom panels) of the collapse of molecular cloud cores with different initial rotation rates. For each panel, the different lines are for cloud cores with $\beta = 0, 5 \times 10^{-4}, 0.001, 0.005, 0.01, 0.04$ from left to right. The free-fall time of the initial cloud core, $t_{\text{ff}} = 1.8 \times 10^{12}$ s (56,500 yrs). Each calculation was performed with 10^6 SPH particles, except the barotropic calculation with $\beta = 0.04$ which used 3×10^5 particles.

constant. The thermal evolution takes into account the translational, rotational, and vibrational degrees of freedom of molecular hydrogen (assuming a 3:1 mix of ortho- and para-hydrogen; see Boley et al. 2007). We also include molecular hydrogen dissociation, and the ionisations of hydrogen and helium. The hydrogen and helium mass fractions are $X = 0.70$ and $Y = 0.28$, respectively. The contribution of metals to the equation of state and the thermal evolution is neglected. Two temperature (gas and radiation) radiative transfer in the flux-limited diffusion approximation is implemented as described by Whitehouse et al. (2005) and Whitehouse & Bate (2006), except that the standard explicit SPH contributions to the gas energy equation due to the work and artificial viscosity are used when solving the (semi-)implicit energy equations to provide better energy conservation. We assume solar metallicity gas, using the interstellar grain opacity tables of Pollack et al. (1985) and the gas opacity tables of Alexander (1975) (the IVa King model) (see Whitehouse & Bate 2006).

2.2 Initial conditions

The initial conditions for the calculations are identical to those of Bate (1998) and Bate (2010). We follow the collapse of initially uniform-density, uniform-rotating, molecular cloud cores of mass $M = 1 M_{\odot}$ and radius $R = 7 \times 10^{16}$ cm. The free-fall time of the initial clouds is $t_{\text{ff}} = 1.785 \times 10^{12}$ s (56,500 yrs). The ratios of the thermal and rotational energies to the magnitude of the gravitational potential energy are $\alpha = 0.54$ and β , respectively. We have performed calculations with $\beta = 0$ (not rotating), and $\beta = 5 \times 10^{-4}, 0.001, 0.005, 0.01$ and 0.04 . Typically, each calculation was performed twice, once using the barotropic equation of state, and again using radiation hydrodynamics.

To satisfy the resolution criterion of Bate & Burkert (1997) that the minimum Jeans mass during the calculation contains at least $\approx 2N_{\text{neigh}} = 100$ particles, we require at least 1×10^5 equal-mass particles. To test for convergence, we performed calculations using $1 \times 10^5, 3 \times 10^5, 1 \times 10^6$, and 3×10^6 equal-mass SPH

β	Equation of State	Number of SPH Particles			
		1×10^5	3×10^5	1×10^6	3×10^6
0	Barotropic			Y	
	Radiation			Y	
0.0005	Barotropic			Y	
	Radiation			Y	
0.001	Barotropic		Y	Y	Y
	Radiation		Y	Y	Y
0.005	Barotropic		Y	Y	
	Radiation	Y	Y	Y	Y
0.01	Barotropic		Y	Y	
	Radiation		Y	Y	
0.04	Barotropic		Y		
	Radiation		Y	Y	

Table 1. A summary of the type of calculations performed, and their numerical resolutions. From left to right, the columns give the type of initial condition (i.e. the values of β , the ratio of the rotational energy to the magnitude of the gravitational potential energy for the molecular cloud cores), the equations of state used (i.e. barotropic equation of state, or radiation hydrodynamics with a realistic equation of state), and which numbers of SPH particles were used to perform calculations.

particles. Only the $\beta = 0.005$ radiation hydrodynamical calculation was performed with all these resolutions, but most calculations were performed with at least two different resolutions (see Table 1). Calculations using the highest resolution of 3×10^6 SPH particles were only performed for the $\beta = 0.001$ cases and radiation hydrodynamical $\beta = 0.005$ case. In this paper, unless otherwise stated, when a particular set of initial conditions and equation of state is discussed or a figure is presented, the calculation performed with the highest resolution is used. We discuss the degree to which the simulations are numerically converged in Appendix A and at various points in Section 3.

The calculations were performed on the University of Exeter Supercomputer, an SGI Altix ICE 8200.

3 RESULTS

The collapse of each molecular cloud core up until the formation of the stellar core proceeds in a manner that is qualitatively similar to those reported from previous three-dimensional calculations without magnetic fields and using barotropic equations of state (Bate 1998; Saigo & Tomisaka 2006; Saigo et al. 2008; Machida et al. 2010; Machida & Matsumoto 2011) for both the barotropic and radiation hydrodynamical calculations presented here.

Fig. 1, gives the evolution with time of the maximum density and temperature for clouds with different initial rotation rates, with each calculation performed using 10^6 particles (except for the barotropic $\beta = 0.04$ case). The initial collapse is isothermal until the maximum density exceeds $10^{-13} \text{ g cm}^{-3}$ using the barotropic equation of state. Using radiation hydrodynamics the evolutions to this density are also almost isothermal. However, slight heating when using radiation hydrodynamics does slow the collapse marginally, leading to the times taken to form the first hydrostatic cores being slightly longer ($\approx 0.01 - 0.015 t_{\text{ff}}$) than in the corresponding barotropic calculations.

In the radiation hydrodynamical calculations, as the heating rate in the central regions exceeds the rate at which the gas can cool, the gas begins to heat up and the collapse enters an almost adiabatic phase where the temperature rises as the gas is compressed.

This is mimicked in the barotropic calculations by the change in the value of η from 1 to 7/5 (equation 1). This increasing temperature leads to the formation of a pressure-supported ‘first hydrostatic core’ (Larson 1969), which can be seen in Fig. 1 when the initial collapse stalls with central (maximum) densities $\sim 10^{-11} \text{ g cm}^{-3}$ and temperatures of $\approx 30 - 120 \text{ K}$, depending on the degree of rotational support (i.e. cores that rotate more quickly have lower maximum temperatures). Again, apart from the small offset in the time of first core formation, the barotropic and radiation hydrodynamical calculations give very similar results to this point.

Without rotation ($\beta = 0$), the first core has an initial mass of ≈ 5 Jupiter masses (M_{J}) and a radius of $\approx 5 \text{ AU}$ (in agreement with Larson 1969). However, with higher initial rotation rates of the molecular cloud core, the first cores become progressively more oblate (Figures 2, 3, and 4). For example, with $\beta = 0.005$ using radiation hydrodynamics, before the onset of dynamical instability, the first core has a radius of $\approx 20 \text{ AU}$ and a major to minor axis ratio of $\approx 4:1$ (first panel in each third row of Figs. 3 and 4). With $\beta = 0.01$, the first core has a radius of $\approx 30 \text{ AU}$ and a major to minor axis ratio of $\approx 6:1$ (fourth rows of these figures). Thus, for the higher rotation rates, the first core is actually a pre-stellar disc, without a central object. As pointed out by Bate (1998), Machida et al. (2010), and Bate (2010), the disc actually forms *before* the star. For the very highest rotation rates ($\beta = 0.04$), the first core actually takes the form of a torus or ring (first panel in each bottom row of Figs. 3 and 4) in which the central density is lower than the maximum density.

3.1 Slowly-rotating first hydrostatic cores

The evolution of the first core up until the point of stellar core formation depends on its rotation rate. Non-rotating and slowly rotating cores evolve as they accrete mass from the surrounding infalling envelope with their central densities and temperatures increasing (Figs. 1 and 5, calculations with $\beta \leq 0.001$). In the radiation hydrodynamical calculations, when the central temperature exceeds $\approx 2000 \text{ K}$, molecular hydrogen begins to dissociate, leading to a second hydrodynamic collapse deep within the first core (Larson 1969). The formation of the stellar core occurs just a few years after the onset of the second collapse, during which the maximum density increases from $\sim 10^{-8}$ to $\gtrsim 0.1 \text{ g cm}^{-3}$ and the maximum temperature increases from ≈ 2000 to $> 60,000 \text{ K}$. The stellar core is formed with a mass of $M_{\text{sc}} \approx 1.5 M_{\text{J}}$ and a radius of $R_{\text{sc}} \approx 2 R_{\odot}$. Without rotation, the stellar core accretes the remnant of the first core in which it is embedded in ≈ 10 years and then accretes the envelope (Larson 1969), though with three-dimensional calculations we only follow the calculations for $\approx 50 - 100$ years after stellar core formation.

Although these stages are qualitatively the same in the barotropic calculations, there is a much greater difference in the evolution of the first core between the barotropic and radiation hydrodynamical calculations than for the phase of the collapse prior to first core formation. To make this clear, in Fig. 5 the time evolution of maximum density and maximum temperature during the calculations is replotted with $t = 0$ set to the time of stellar core formation (defined as the time when the maximum density reaches $10^{-3} \text{ g cm}^{-3}$). This allows us to clearly see the amount of time spent between first core formation and stellar core formation in each of the calculations. The barotropic results are plotted using dashed lines, while the solid lines give the radiation hydrodynamical results. The evolution time of the first core or pre-stellar disc is longer using radiation hydrodynamics than using the barotropic

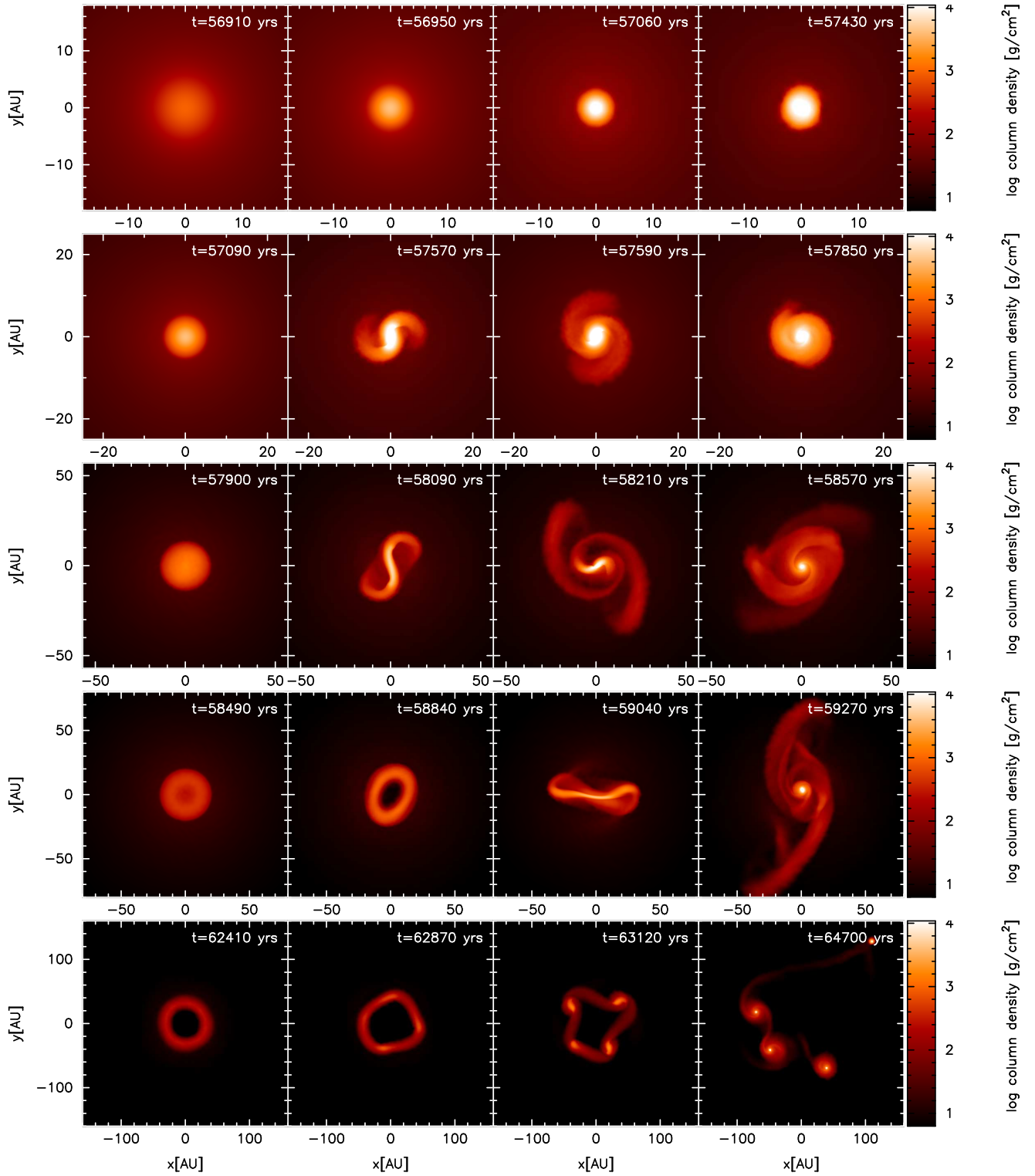


Figure 2. Snapshots of the column density viewed parallel to the rotation axis during the evolution of the barotropic calculations of the collapse of molecular cloud cores with different initial rotation rates. From top to bottom, the different rows are for cloud cores with $\beta = 5 \times 10^{-4}$, 0.001, 0.005, 0.01, 0.04. Note that the spatial scale is different for each row, with each panel measuring $1600\sqrt{\beta}$ AU across (i.e. from 36 to 320 AU). The free-fall time of the initial cloud core, $t_{\text{ff}} = 1.8 \times 10^{12}$ s (56,500 yrs). Each calculation was performed with 10^6 SPH particles, except for the $\beta = 0.001$ case which used 3×10^6 SPH particles and the $\beta = 0.04$ case which used 3×10^5 particles. The evolution is almost identical when using 3×10^5 particles or more, but the latter are slightly more detailed.

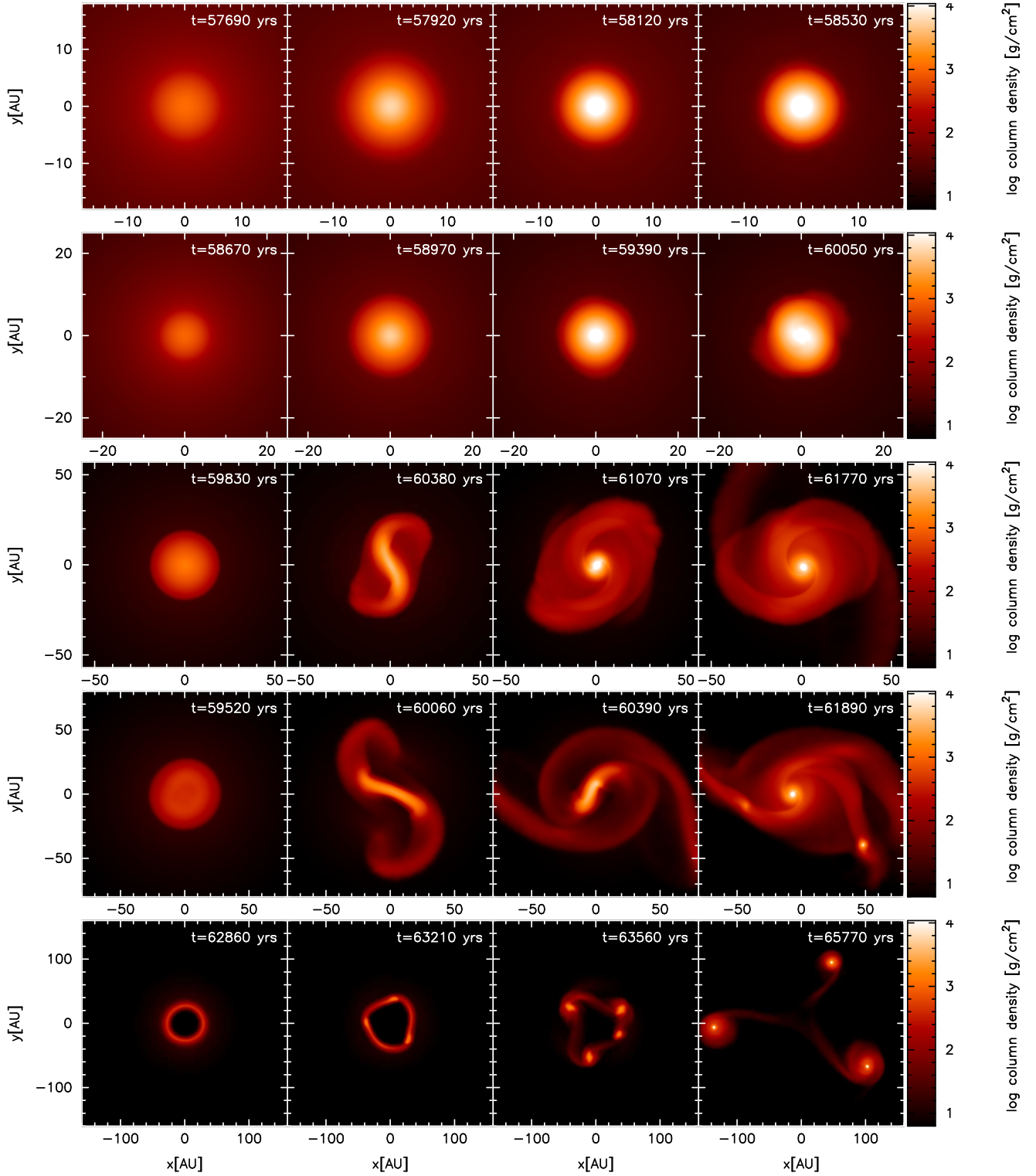


Figure 3. Snapshots of the column density viewed parallel to the rotation axis during the evolution of the radiation hydrodynamical calculations of the collapse of molecular cloud cores with different initial rotation rates. From top to bottom, the different rows are for cloud cores with $\beta = 5 \times 10^{-4}, 0.001, 0.005, 0.01, 0.04$. Note that the spatial scale is different for each row, with each panel measuring $1600\sqrt{\beta}$ AU across (i.e. from 36 to 320 AU). The free-fall time of the initial cloud core, $t_{\text{ff}} = 1.8 \times 10^{12}$ s (56,500 yrs). Each calculation was performed with 10^6 SPH particles, except for the $\beta = 0.001$ and $\beta = 0.005$ cases which used 3×10^6 SPH particles. The evolution is almost identical when using 10^6 or 3×10^6 particles, but the latter are slightly more detailed (see Appendix A).

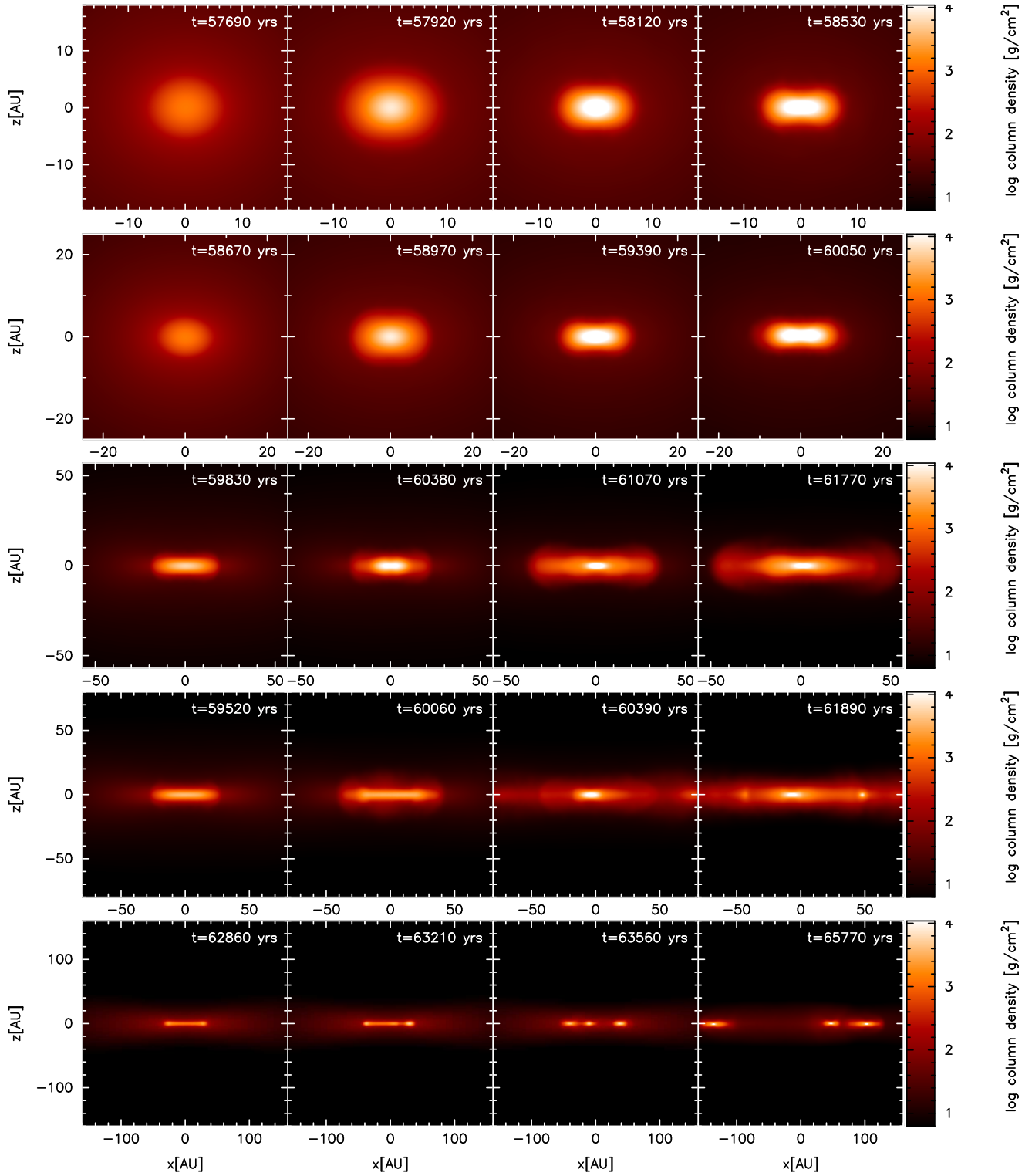


Figure 4. Snapshots of the column density viewed perpendicular to the rotation axis during the evolution of the radiation hydrodynamical calculations of the collapse of molecular cloud cores with different initial rotation rates. From top to bottom, the different rows are for cloud cores with $\beta = 5 \times 10^{-4}$, 0.001, 0.005, 0.01, 0.04. Note that the spatial scale is different for each row, with each panel measuring $1600\sqrt{\beta}$ AU across (i.e. 36, 50, 114, 160, or 320 AU). The free-fall time of the initial cloud core, $t_{\text{ff}} = 1.8 \times 10^{12}$ s (56,500 yrs). Each calculation was performed with 10^6 SPH particles, except for the $\beta = 0.001$ and $\beta = 0.005$ cases which used 3×10^6 SPH particles. The evolution is almost identical when using 10^6 or 3×10^6 particles, but the latter are slightly more detailed (see Appendix A).

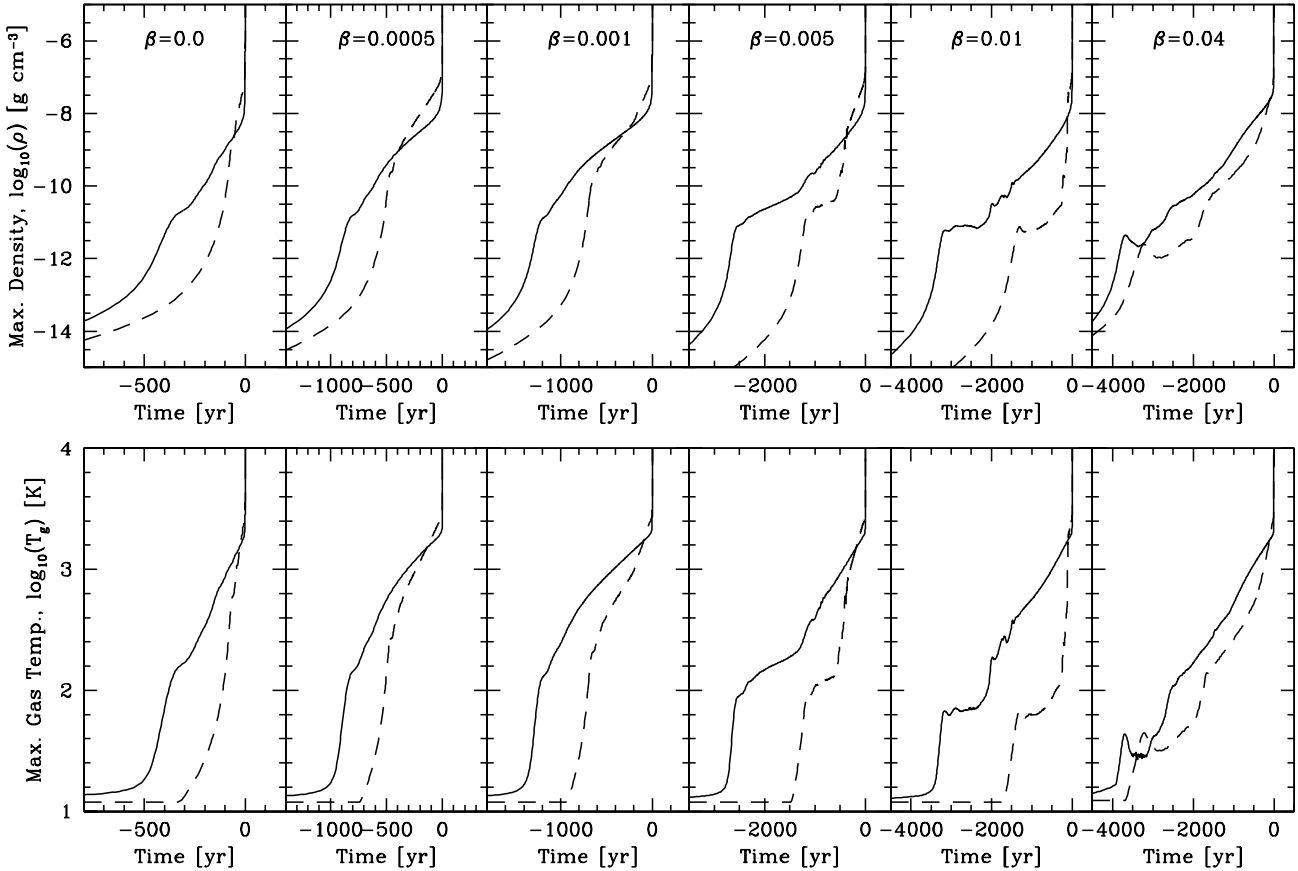


Figure 5. The time evolution of the maximum density (upper panels) and gas temperature (lower panels) during the radiation hydrodynamical calculations of the collapse of molecular cloud cores with different initial rotation rates. From left to right, the different panels are for cloud cores with $\beta = 0, 5 \times 10^{-4}, 0.001, 0.005, 0.01, 0.04$. The dashed lines give the evolution using the barotropic equation of state, while the solid lines give the evolution using radiation hydrodynamics. Time is set to zero at the end of the second dynamic collapse phase when the density reaches $10^{-3} \text{ g cm}^{-3}$ which allows the length of the first hydrostatic core phases to be compared. It can be seen that the length of the first core phase increases with increasing rotation rate, but also that the use of radiation hydrodynamics and a realistic equation of state lengthens the first core phase relative to calculations that use the barotropic equation of state. Each calculation was performed with 10^6 SPH particles, except the barotropic calculation with $\beta = 0.04$ which used 3×10^5 particles.

equation of state in all cases, by factors of $1.5 - 3$ except for the most rapidly-rotating case. This is because the barotropic equation of state consistently underestimates the temperature of the gas, providing less pressure support to the gas and, thus, allowing it to enter the second collapse phase earlier. The consistent temperature underestimate can be seen clearly in Fig. 6 which plots the maximum temperature versus maximum density for each of the radiation hydrodynamical calculations and compares this to the barotropic equation of state (dashed black solid line). The lines from the radiation hydrodynamical calculations almost lie on top of one another, but from densities of 10^{-11} to $10^{-8} \text{ g cm}^{-3}$ the barotropic equation of state underestimates the maximum temperature by about a factor of two. The only exception to this is the most rapidly-rotating calculation with $\beta = 0.04$. Here the maximum temperature at a given density is lower than in the other radiation hydrodynamical calculations and more similar to the barotropic equation of state. This is because in this case the first core is actually a torus and, therefore, the gas can cool more effectively. Returning to Fig. 5, we also see that it is the $\beta = 0.04$ case (rightmost panels) where the timescales between first and stellar core formation are most similar for the barotropic and radiation hydrodynamical calculations (differing only by about 15% rather than a factor of $1.5 - 3$).

One possible reason that the radiation hydrodynamical calculations give greater temperatures during the first core phase than the barotropic calculations is that there may be considerable shock heating which is not taken into account with a barotropic equation of state. However, computing the entropy of the gas before the first core forms and in the bulk of the first core as it forms and evolves, we find it monotonically decreases in the radiation hydrodynamical calculations. The rate of decrease is rapid before the first core forms (when it is cooling rapidly and almost isothermal), but even after the first core forms the gas is losing energy due to radiation. Only at the surface of the first core (around the accretion shock) does the entropy briefly increase before it radiatively cools. This is consistent with the recent calculations of Commerçon et al. (2011) who find that essentially all of the energy liberated in the accretion shock is radiated away.

Instead, the reason the barotropic equation of state consistently underestimates the temperature in this density range is due to the approximation that $\eta = 7/5$ in this part of the evolution. In fact, molecular hydrogen (the dominant constituent) has a ratio of specific heat capacities of $\gamma = 5/3$ until it reaches $\sim 100 \text{ K}$. Only then are the rotational degrees of freedom, which lower γ to $7/5$, excited. Again, this is apparent in Fig. 6 where it can be seen that the lines

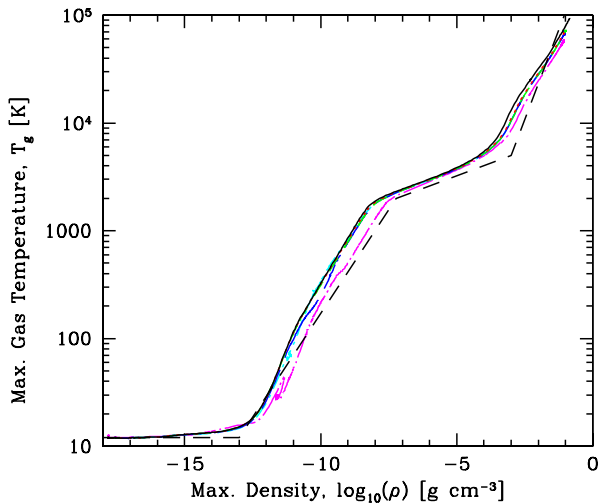


Figure 6. The evolution of the maximum gas temperature versus maximum density for the radiation hydrodynamical collapse of molecular cloud cores with $\beta = 0$ (solid black line), 5×10^{-4} (dotted red curve), 0.001 (short-dashed green curve), 0.005 (long-dashed blue curve), 0.01 (dot-short dashed cyan curve), 0.04 (dot-long-dashed magenta curve). The barotropic equation of state is given by the black short-dashed lines. The axisymmetric ($\beta = 0$) case is always the hottest at a given maximum density because the radiation is most effectively trapped. Conversely, the calculation that is the coolest has the highest rotation rate ($\beta = 0.04$). Each calculation was performed with 10^6 SPH particles.

from the radiation hydrodynamical calculations are steeper than the barotropic line in the temperature range $\approx 20 - 150$. Above this temperature, the lines are almost parallel (i.e. $\gamma \approx 7/5$ for both), but the temperature offset (that originates in the $20 - 150$ K range) persists. The barotropic equation of state could be improved for this part of the evolution by including a smooth transition from $\gamma = 1$ to $5/3$ and then a transition from $5/3$ to $7/5$. However, this would still not capture all of the detail present in the radiation hydrodynamical equations (see below).

3.2 Rotationally-unstable first hydrostatic cores

If the first core is rotating rapidly enough that its own value of $\beta > 0.274$, the core is dynamically unstable to the growth of non-axisymmetric structure (Bate 1998; Machida et al. 2005; Saigo & Tomisaka 2006; Saigo et al. 2008; Bate 2010; Machida et al. 2010; Tomida et al. 2010; Saigo & Tomisaka 2011; Machida & Matsumoto 2011). For the particular initial conditions used here, this occurs for the $\beta = 0.001 - 0.01$ cases (see Figs. 2 and 3). The torus that forms in the $\beta = 0.04$ calculations is also dynamically unstable, but this case is somewhat different and will be discussed further below.

In each of the $\beta = 0.001 - 0.005$ cases, the first core begins as an axisymmetric flattened pre-stellar disc, but after several rotations it develops a bar-mode (e.g. the second panel of the third row in each of Figures 2 and 3). The ends of the bar subsequently lag behind and the bar winds up to produce a spiral structure. Spiral structure removes angular momentum from the inner parts of the first core via gravitational torques (Bate 1998), the effect of which can be seen in the evolution of density and temperature in Fig. 5. For example, in the $\beta = 0.005$ case, the slow increases

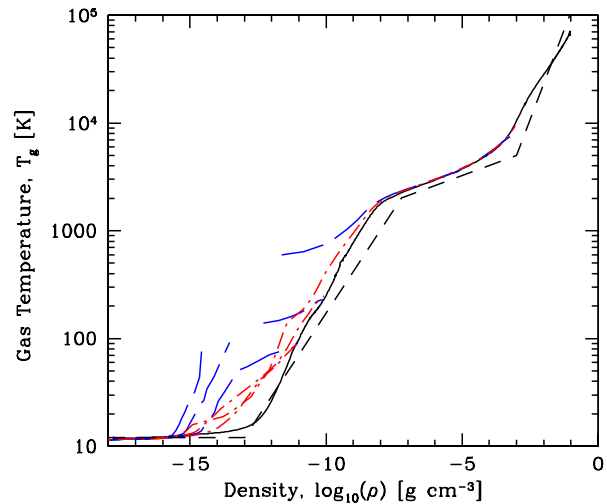


Figure 7. For the radiation hydrodynamical collapse of the molecular cloud core with $\beta = 0.005$, we give the evolution of the maximum gas temperature versus maximum density during the collapse (solid black curve) and snapshots of gas temperature versus density along the rotation (z) axis (long-dashed blue curves) and perpendicular to the rotation axis (dot-dashed red curves) at three different times. Note that the long-dashed blue lines at higher temperatures (later times) have a break in them. This is because there is not enough gas along the rotation axis at these densities to determine an accurate temperature. These densities occur within the accretion shock onto the first core. Although the evolution of the maximum temperature versus maximum density is similar to that given by the barotropic equation of state (black short-dashed lines), the gas temperature surrounding the protostar tends to be much hotter at a given density than predicted by the barotropic equation of state, particularly along the rotation axis where the temperatures can be more than an order of magnitude hotter. This calculation was performed with 3×10^6 SPH particles.

in central density and temperature after first core formation suddenly accelerate with the onset of the spiral structure. This occurs at about 1300 yrs before stellar core formation for the radiation hydrodynamical calculation with $\beta = 0.005$ and about 600 yrs before stellar core formation for the barotropic calculation. Similar accelerations are seen for both the $\beta = 0.01$ cases and also for the barotropic $\beta = 0.001$ case. Thus, the removal of angular momentum from the central regions of the core substantially accelerates the evolution of the first core towards the second collapse, which would take much longer to reach without the angular momentum redistribution (i.e. due to accretion and radiative cooling alone).

In Figs. 2 and 3, the development of the spiral structure and the subsequent concentration of material towards the centre of the core due to the redistribution of angular momentum is clearly visible for the barotropic cases with $\beta = 0.001 - 0.01$ and the radiation hydrodynamical cases with $\beta = 0.005 - 0.01$. In Fig. 8 we also provide the density-weighted temperature, for comparison with the column density in Fig. 3. As gas is concentrated to the centre of the cores its temperature greatly increases. It is also apparent that the spiral shocks in the discs are hotter than the rest of the discs.

The barotropic and radiation hydrodynamical evolutions are qualitatively similar in that both display the progression from an axisymmetric core, to bar instability, to a torus as the initial rotation rate of the molecular cloud core is increased. However, radiation hydrodynamical calculations are more resistant to the bar instability than the barotropic calculations. This is directly attributable to

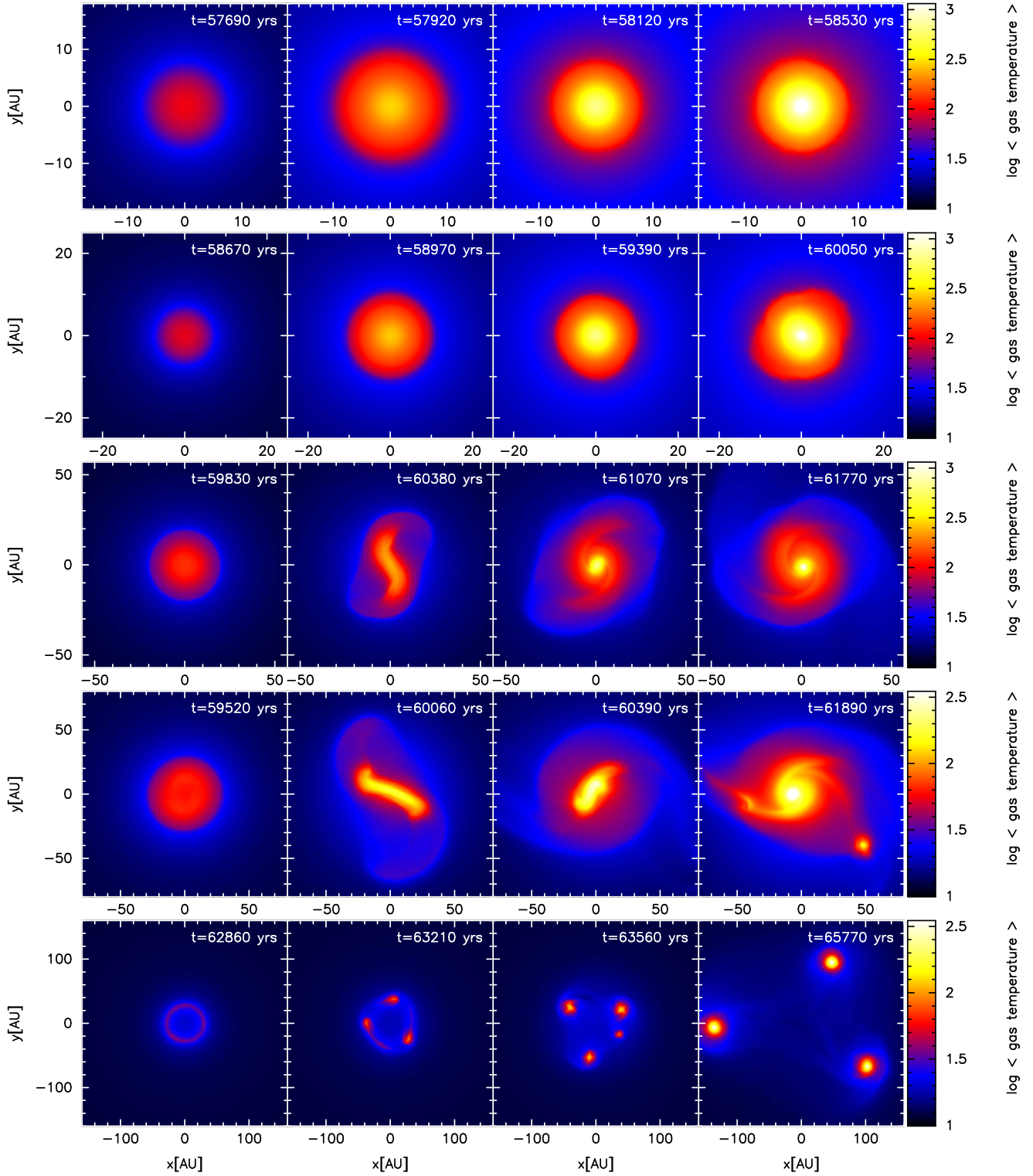


Figure 8. Snapshots of the density-weighted temperature viewed parallel to the rotation axis during the evolution of the radiation hydrodynamical calculations of the collapse of molecular cloud cores with different initial rotation rates. From top to bottom, the different rows are for cloud cores with $\beta = 5 \times 10^{-4}$, 0.001, 0.005, 0.01, 0.04. Note that the spatial scale is different for each row, with each panel measuring $1600\sqrt{\beta}$ AU across (i.e. from 36 to 320 AU). The temperature scale differs between the top three rows and the lower two rows in order to enhance the low-temperature structure in the cases with greater rotation. The free-fall time of the initial cloud core, $t_{\text{ff}} = 1.8 \times 10^{12}$ s (56,500 yrs). Each calculation was performed with 10^6 SPH particles, except for the $\beta = 0.001$ and $\beta = 0.005$ cases which used 3×10^6 SPH particles. The evolution is almost identical when using 10^6 or 3×10^6 particles, but the latter are slightly more detailed (see Appendix A).

the difference in the thermal evolution of the gas that was discussed above. Since the gas is somewhat hotter in the radiation hydrodynamical calculations, the first core is larger (more ‘puffy’) and has a lower value of β for a given β value of the initial molecular cloud core. Tomida et al. (2010) also noticed that the first cores in their radiation magnetohydrodynamical calculations had higher entropies and larger sizes than when they used a barotropic equation of state. It should be noted, however, that with radiation hydrodynamics there is no one-to-one relation between temperature and density (see also Boss et al. 2000; Whitehouse & Bate 2006; Tomida et al. 2010). This is illustrated in Fig. 7, where we plot temperature versus density from various snapshots from the $\beta = 0.005$ calculation and compare this to both the run of maximum temperature versus maximum density during the calculation and the barotropic equation of state. The red dot-dashed lines are for cuts perpendicular to the rotation axis along the x -axis (i.e. in the plane of the disc), while the blue long-dashed lines display the temperature along the rotation axis. Not only is the run of maximum temperature versus maximum density always greater than or equal to the temperature from the barotropic equation of state, but the gas both in the mid-plane of the disc and along the rotation axis at the same density is even hotter. This is particularly true of the gas along the rotation axis, which is heated by the accretion shock at the surface of the first core. Tomida et al. (2010) give a very similar plot for a snapshot from one of their simulations and find very similar behaviour.

These hotter temperatures in the radiation hydrodynamical calculations mean that while the transition from rotationally stable to dynamically unstable first core occurs in the range $\beta = 5 \times 10^{-4} - 10^{-3}$ using the barotropic equation of state, the transition occurs at $\beta \approx 0.001$ with radiation hydrodynamics (this case undergoes an extremely weak instability, just visible in the fourth panel of the second row of Fig. 3). Similarly, while the barotropic calculation with $\beta = 0.01$ manages to produce a torus-shaped first core, the radiation hydrodynamical calculation with $\beta = 0.01$ is still definitely disc shaped rather than torus shaped.

As mentioned above, for the highest initial rotation rates ($\beta = 0.04$) the first core is actually a torus or ring-like structure (e.g. Norman & Wilson 1978; Cha & Whitworth 2003; Machida et al. 2005). Such a configuration is highly unstable to non-axisymmetric perturbations and, indeed, as is clearly visible in Figs. 2 and 3 the rings rapidly fragment into four objects. Such a configuration is highly chaotic, and symmetry is broken quickly (due to truncation error and the use of a tree-structure to calculate gravity in the calculations). In the radiation hydrodynamical calculation, two of the fragments merge to produce a triple system, while in the barotropic calculation all four fragments survive (at least until the calculation was stopped). Each of the fragments follows its own evolution toward the second collapse phase and stellar core formation. The calculations were stopped soon after the first fragment in each calculation produced a stellar core.

Finally, as mentioned above, first cores may evolve into pre-stellar discs with radii ranging from ≈ 5 to $\gtrsim 100$ AU before a stellar core forms (Fig. 3). Those with radii greater than ≈ 10 AU are produced due to the angular momentum transport that occurs during the dynamical rotational instability. A further consequence is that all star formation should go through at least a brief phase when the disc mass is greater than the stellar mass. Such discs are gravitationally unstable and may evolve through spiral density waves (e.g. the third row of Figs. 3 and 8) and/or fragmentation (e.g. the fourth rows of Fig. 3 and 8). This is discussed further in Section 4.

In conclusion, in switching from the simple barotropic equation of state to a realistic equation of state with radiation hydro-

namics, the qualitative evolution of the first core and its dependence on the initial rotation rate of the molecular cloud core is identical. However, the gas temperature in the more realistic calculations tends to be hotter and is not only a function of density: for example, the gas is significantly hotter in the accretion shock at the surface of the first cores. Quantitatively, the higher temperatures mean that the critical values of the initial molecular cloud core rotation rates required for bar instability of the first core, or the transition to a torus geometry is somewhat higher. The value of β must be $\approx 50\%$ greater with radiation hydrodynamics, which translates into a rotation rate which is $\approx 25\%$ greater (since $\beta \propto \Omega^2$, where Ω is the angular frequency of the molecular cloud core).

3.3 The effect of stellar core formation

Although the evolution of the first core or pre-stellar disc is qualitatively the same when computed with a barotropic equation of state or radiation hydrodynamics, as Bate (2010) showed the evolution subsequent to the formation of the stellar core is *qualitatively different*. When using a barotropic equation of state, the formation of the stellar core deep within the optically-thick disc has no effect on the temperature of the gas further out in the disc because its temperature is set purely according to its density. However, with radiation hydrodynamics, the situation is completely different.

When the second collapse occurs and produces the stellar core, the gravitational potential energy that is released is $\sim GM_{sc}^2/R_{sc} = 4 \times 10^{42}$ erg. Since the stellar core is in virial equilibrium, approximately half of this energy is radiated away. Moreover, the stellar core rapidly begins to accrete from the first core, reaching a mass of $\approx 6 M_J$ in only a few years (i.e. more quickly than the dynamical timescale of the large-scale disc; see below). This increases the total energy released to $\approx 3 \times 10^{43}$ erg. Bate (2010) compared this energy with the binding energy of the disc in the $\beta = 0.005$ calculation. Just before the onset of the second collapse, the binding energy of the pre-stellar disc is only 4×10^{43} erg (estimated as $\sim GM_d^2/R_d$ with $M_d \approx 0.18 M_\odot$ and taking a mean ‘spherical’ radius of $R_d \approx 15$ AU). Thus, when the second collapse occurs, the disc suddenly finds itself irradiated from the inside by an energy source emitting a substantial fraction of the binding energy of the disc itself. Because the disc is extremely optically thick, this energy is temporarily trapped in the centre of the disc and heats the gas dramatically, sending a weak shock wave out along the midplane of the disc at a speed of a few km s^{-1} . However, perpendicular to the disc, the effect is even more dramatic. Because there is less material along the rotation axis, the hot gas finds it easiest to break out in this direction and a bipolar outflow is launched. Whereas the wave within the disc decays as it travels leaving the bulk of the disc gravitationally bound, the gas forming the bipolar outflow has velocities up to 10 km s^{-1} and travels out into the infalling envelope to distances in excess of 50 AU in less than 50 years. Using two-dimensional radiation hydrodynamical calculations, Schönke & Tscharnuter (2011) have recently reported similar behaviour, although the outflow in their simulations is less bipolar. By disregarding the central regions of one of their calculations, they were able to follow the outflow for a few tens of thousands of years and found that after reaching ≈ 500 AU, the material fell back in to reform a disc.

Bate (2010) mainly discussed the $\beta = 0.005$ calculation as typical example. Here we examine how the effect of stellar core formation on the surrounding disc depends on the initial rotation rate of the molecular cloud core and, thus, on the degree of rotation that the first core/pre-stellar disc has. Figs. 9 to 14 illustrate the

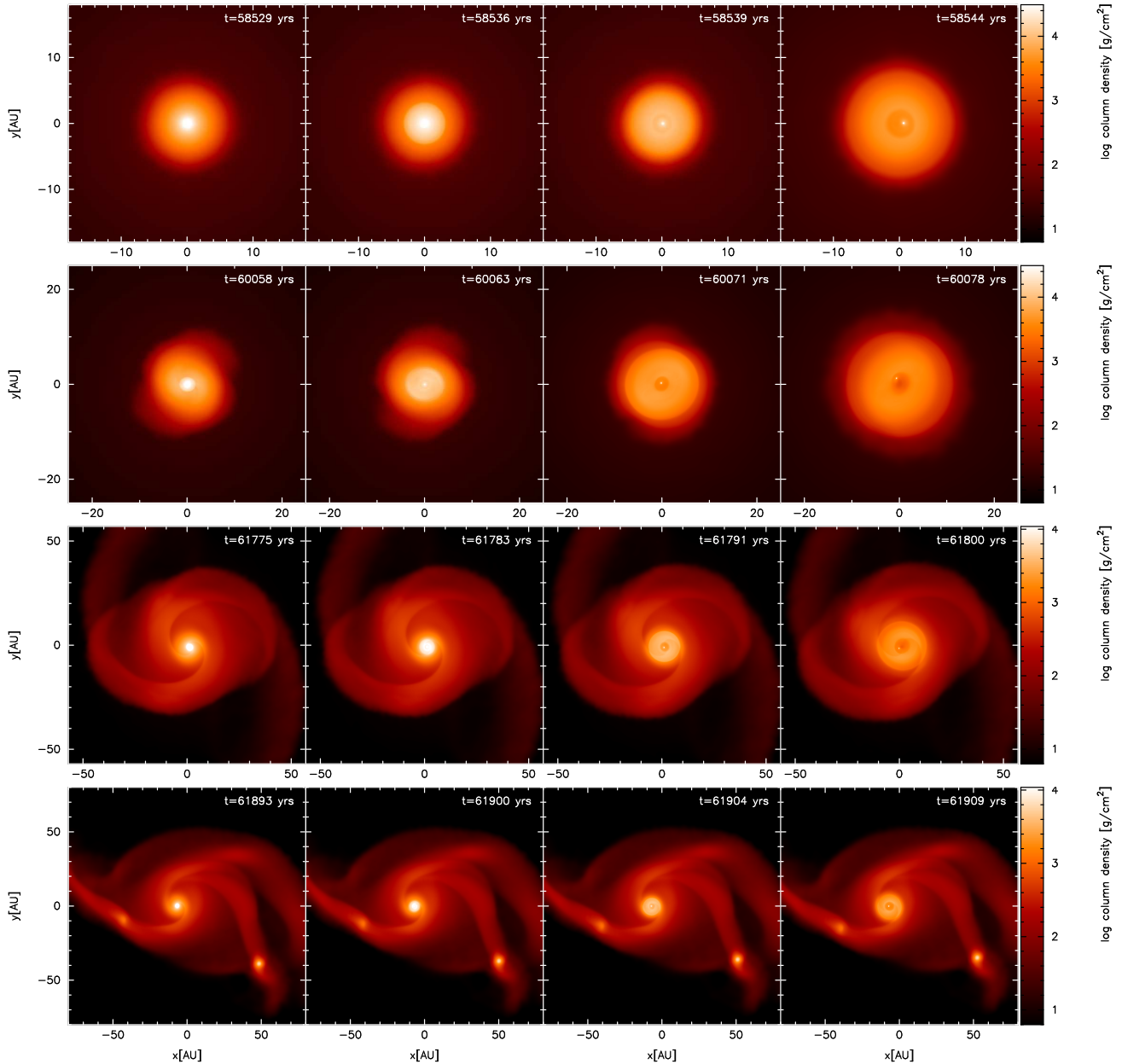


Figure 9. Snapshots of the column density viewed parallel to the rotation axis during the evolution of the radiation hydrodynamical calculations of the collapse of molecular cloud cores with different initial rotation rates. The shockwaves propagating outwards through the discs following stellar core formation are clearly visible. From top to bottom, the different rows are for cloud cores with $\beta = 5 \times 10^{-4}$, 0.001, 0.005, 0.01, 0.04. Note that the spatial scale is different for each row, with each panel measuring $1600\sqrt{\beta}$ AU across (i.e. from 36 to 320 AU). The free-fall time of the initial cloud core, $t_{\text{ff}} = 1.8 \times 10^{12}$ s (56,500 yrs). Each calculation was performed with 10^6 SPH particles, except for the $\beta = 0.001$ and $\beta = 0.005$ cases which used 3×10^6 SPH particles. The evolution is almost identical when using 10^6 or 3×10^6 particles, but the latter are slightly more detailed (see Appendix A).

evolution of calculations with $\beta = 5 \times 10^{-4} - 0.01$ following stellar core formation. The $\beta = 0$ case is not discussed further since the situation is as Larson (1969) described it. This case remains spherically-symmetric, and although the stellar core irradiates the first core from within, the radiation liberated is not sufficient to stop the spherically-symmetric accretion flow onto the stellar core. We do not discuss the $\beta = 0.04$ case following stellar core formation since each of the three fragments is qualitatively similar to the first core obtained in the $\beta = 0.001$ case and, therefore, we assume that each of these cores would evolve in a similar manner.

Figs. 9 and 10 provide snapshots of the column density in the directions parallel to the rotation axis and perpendicular to the rotation axis, respectively. The shockwave propagating outwards through each of the first cores/discs is clearly visible in Fig. 9. For the $\beta = 5 \times 10^{-4}$ and 0.001 cases, the shockwave reaches the outer edge of the disc before the calculations are stopped. For the $\beta = 0.005$ and 0.01 cases, we were not able to follow the calculations this long and the shockwave was only followed 10–15 AU. In Fig. 10, both the propagation of the shockwaves through the discs and the bipolar outflows launched perpendicular to the discs are

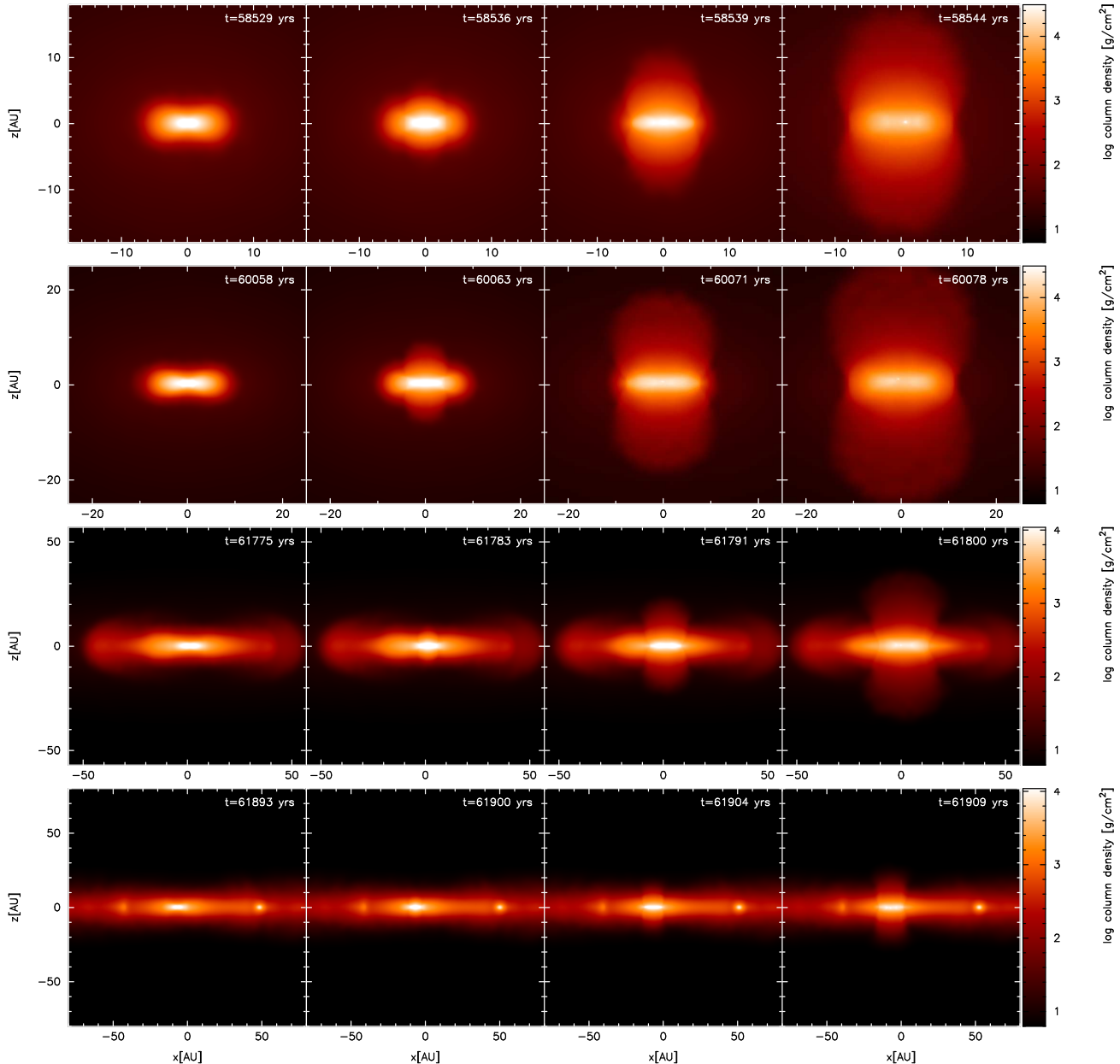


Figure 10. Snapshots of the column density viewed perpendicular to the rotation axis during the evolution of the radiation hydrodynamical calculations of the collapse of molecular cloud cores with different initial rotation rates. The bipolar outflows, launched after stellar core formation, are clearly visible. From top to bottom, the different rows are for cloud cores with $\beta = 5 \times 10^{-4}$, 0.001, 0.005, 0.01, 0.04. Note that the spatial scale is different for each row, with each panel measuring $1600\sqrt{\beta}$ AU across (i.e. 36, 50, 114, 160, or 320 AU). The free-fall time of the initial cloud core, $t_{\text{ff}} = 1.8 \times 10^{12}$ s (56,500 yrs). Each calculation was performed with 10^6 SPH particles, except for the $\beta = 0.001$ and $\beta = 0.005$ cases which used 3×10^6 SPH particles. The evolution is almost identical when using 10^6 or 3×10^6 particles, but the latter are slightly more detailed (see Appendix A).

clearly visible, the latter reaching to distances of 15–35 AU. The furthest an outflow was followed was to a distance of 60 AU in the $\beta = 0.005$ case, approximately 50 years after the outflow began (Bate 2010).

Each of Figs. 11 to 13 give density, velocity, and temperature profiles, both in the disc plane and perpendicular to the disc plane (i.e. along the rotation axis), at four characteristic times during the evolution following stellar core formation. They also provide the radial mass profiles. Fig. 11 shows the evolution of the barotropic $\beta = 0.005$ calculation which can be compared with the results

from the radiation hydrodynamical calculations in Figs. 12 to 13 with $\beta = 5 \times 10^{-4}$ and 0.005. We do not provide figures for $\beta = 0.001$ and 0.01 since they are qualitatively similar to the cases with $\beta = 5 \times 10^{-4}$ and 0.005, respectively.

In all calculations, the stellar core forms with a radius of $R_{\text{sc}} \approx 0.01$ AU (i.e. $\approx 2R_{\odot}$) and a mass of a few M_{J} (e.g. Fig. 11, top-left and top-centre panels). Using the barotropic equation of state (Fig. 11), the radii of the first core (actually a disc) and stellar core are clearly visible in the top-centre panel which gives the radial velocity profiles just after stellar core formation. Gas falling on

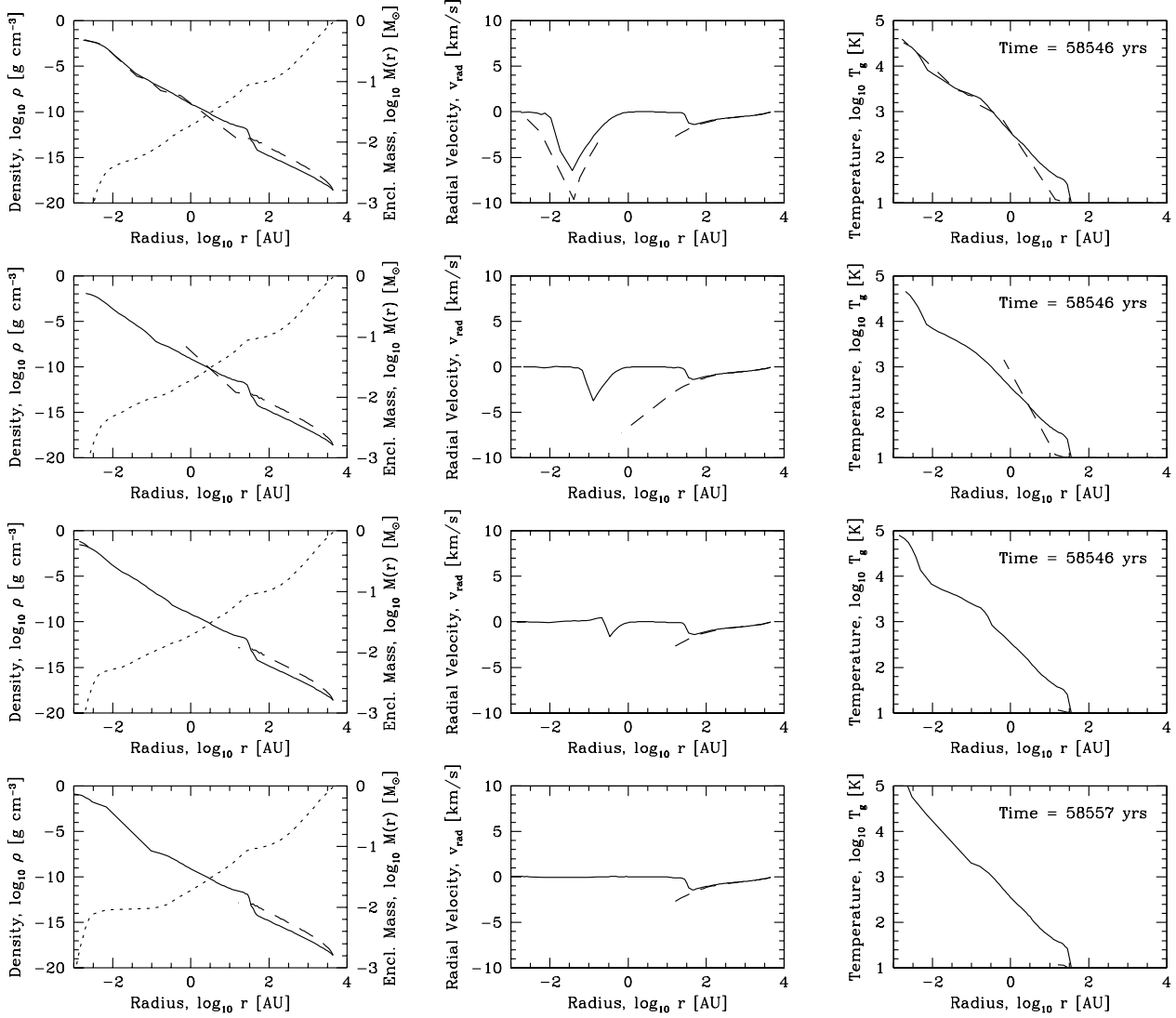


Figure 11. The evolution of the barotropic $\beta = 0.005$ calculation of the collapse of a molecular cloud core following stellar core formation. Each of the four rows shows the state of the protostar at different time. The left panels provide the radial density profile perpendicular to the rotation axis (solid line, averaged in azimuth), the density profile along the rotation axis (dashed line), and the cumulative mass profile (dotted line). The centre panels give the radial velocity profiles perpendicular to (solid line) or along (dashed line) the rotation axis. The right panels show the radial temperature profiles perpendicular to (solid line) or along (dashed line) the rotation axis. Breaks in the lines occur when there is not sufficient gas resolution to define an accurate measurement.

to the first core from the envelope at speeds of $\approx 2 - 4 \text{ km s}^{-1}$ is visible at radii of $\approx 10 - 30 \text{ AU}$, while gas falling onto the stellar core much more rapidly (up to $7 - 10 \text{ km s}^{-1}$) is apparent at radii of $\approx 0.01 - 0.3 \text{ AU}$. In less than a year (second and third rows of Fig. 11), an inner disc builds up around the stellar core (radius $\approx 0.07 \text{ AU}$ in the centre panel of the second row, and $\approx 0.2 \text{ AU}$ in the centre panel of the third row) and the radial extent of the region undergoing dissociation and collapse on to the stellar core and inner disc is reduced. Several years after the stellar core has formed (bottom row of Fig. 11), the outer edge of the inner disc has completely merged into the outer disc (the remnant of the first core) and the azimuthally-averaged radial velocity in the disc plane is approximately zero out to $\approx 30 \text{ AU}$. The formation of an inner disc around the stellar core, which grows in radius as gas with higher angular momentum falls in through the region of molecular hydrogen dissociation, and the eventual merger of the inner and outer discs is just as was first discussed by Bate (1998), and more recently stud-

ied by Machida et al. (2010) and Machida & Matsumoto (2011) who also included magnetic fields.

Using radiation hydrodynamics, the evolution is initially similar to the barotropic cases. For example, take the $\beta = 5 \times 10^{-4}$ case (Fig. 12). In the top-centre panel, the first core and stellar cores are clearly visible in the radial velocity profiles due to the accretion shocks at their surfaces. An inner disc builds up around the stellar core as material with higher angular momentum falls inwards and the radial extent of the dissociating, collapsing region decreases (centre panel of the second-row).

However, as the inner disc grows in radius and begins to merge with remnant of the first core, a bipolar outflow is launched vertically at about 5 km s^{-1} (dashed line in the centre panel of the third-row of Fig. 12), while a lower-velocity shock propagates outward along the disc mid-plane at $\approx 1 \text{ km s}^{-1}$. All of this evolution occurs within just 4 – 5 years of the stellar core forming. At 20 years after stellar core formation, the outflow has travelled more than 20 AU

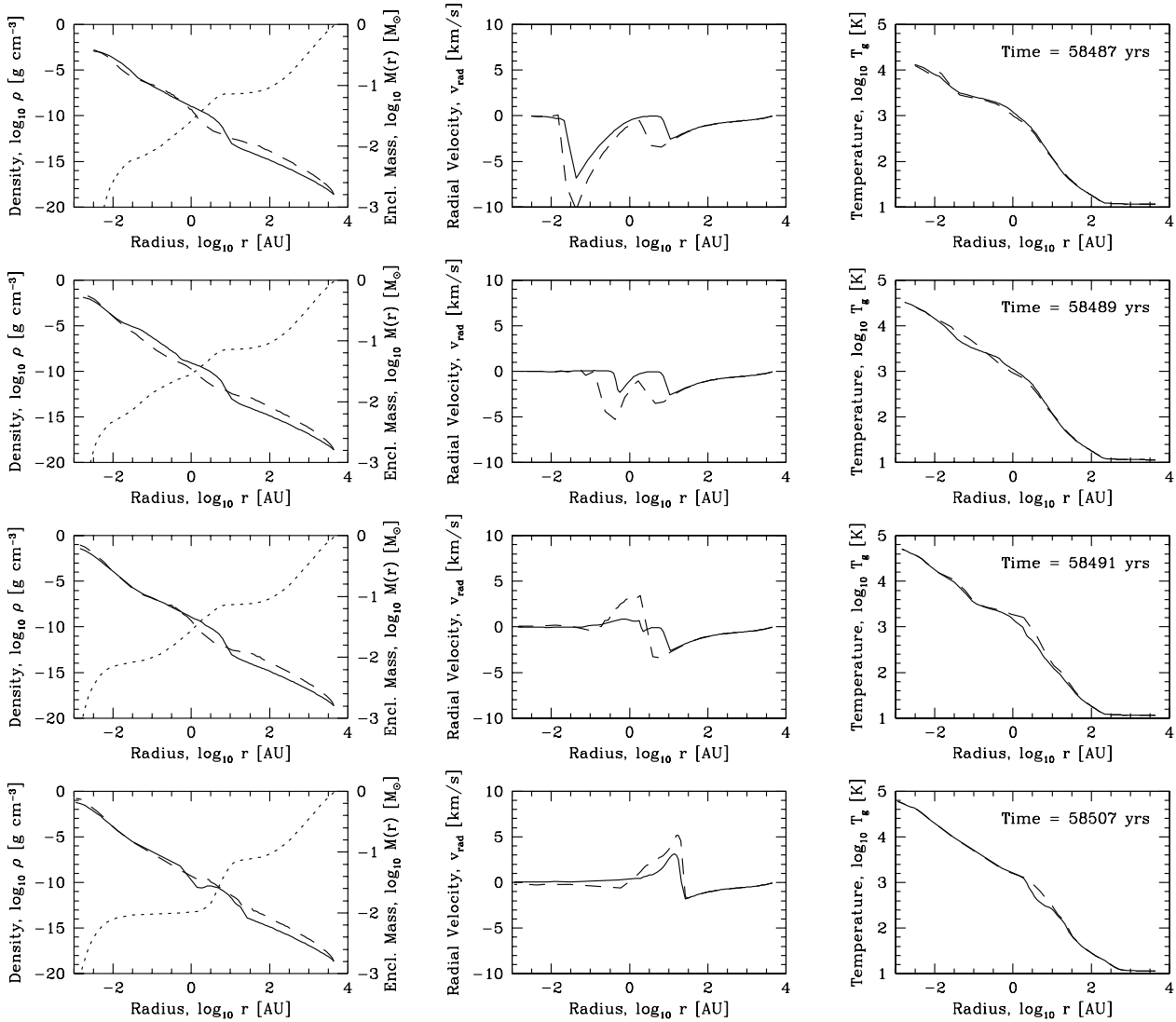


Figure 12. The evolution of the radiation hydrodynamical $\beta = 5 \times 10^{-4}$ calculation of the collapse of a molecular cloud core following stellar core formation. Each of the four rows shows the state of the protostar at different time. The left panels provide the radial density profile perpendicular to the rotation axis (solid line, averaged in azimuth), the density profile along the rotation axis (dashed line), and the cumulative mass profile (dotted line). The centre panels give the radial velocity profiles perpendicular to (solid line) or along (dashed line) the rotation axis. The right panels show the radial temperature profiles perpendicular to (solid line) or along (dashed line) the rotation axis.

and the shockwave in the disc has burst out of the edge of the disc (centre panel of the bottom-row of Fig. 12; see also Fig. 10).

The outflow and the shockwave do not vary greatly with the degree of rotation of the first core/pre-stellar disc (c.f. Figs. 12 and 13). In all cases, the outflow is launched (vertically) at a radius of ≈ 0.5 AU from the stellar core, just before the outer edge of the inner disc merges (in the disc plane) with the remnant of the first core/pre-stellar disc at ≈ 1 AU and the infalling region of dissociating molecular hydrogen disappears (e.g. the centre panel of the second row in Fig. 13). The peak speed of the outflow is slightly larger when the first core is rotating more rapidly, ranging from ≈ 5 km s $^{-1}$ for the $\beta = 5 \times 10^{-4}$ case to ≈ 10 km s $^{-1}$ for the $\beta = 0.01$ case. The outflows have been followed for long enough in the $\beta = 0.001$ and $\beta = 0.005$ calculations (to distances of 30 and 60 AU, respectively) that speeds of the outflows were clearly seen to decay (c.f. the dashed lines in the centre panels of the third and fourth rows of Fig. 13). This outflowing material will not leave the system; it will eventually stall and fall back onto the proto-

star and disc (Schönke & Tschamner 2011). It is worth noting that because the flux-limited diffusion method used to calculate the radiative transfer in the calculations presented here assumes that the material radiates with maximal efficiency, it may overestimate the cooling and hence underestimate the temperatures in the optically-thin outflowing material. Thus, the outflow may be even stronger with a more accurate method of radiative transfer.

The shockwave propagating outwards through the disc travels with a speed of $1 - 2$ km s $^{-1}$ in all cases. In the $\beta = 5 \times 10^{-4}$ and $\beta = 0.001$ calculations, the shockwave is followed until after it has reached the edge of the first core/pre-stellar disc. The combination of the outflow and the outward propagating wave in the disc plane evacuate most of the gas from within a few AU of the protostar, leaving the stellar core surrounded by a broad torus, rather than a disc. This is apparent in the column density plots in Fig. 9, as well as the mass and density profiles in the bottom rows of Figs. 12 to 13. These holes would eventually fill in again as the disc evolves. In the low-resolution calculations, the mass resolution is poor and

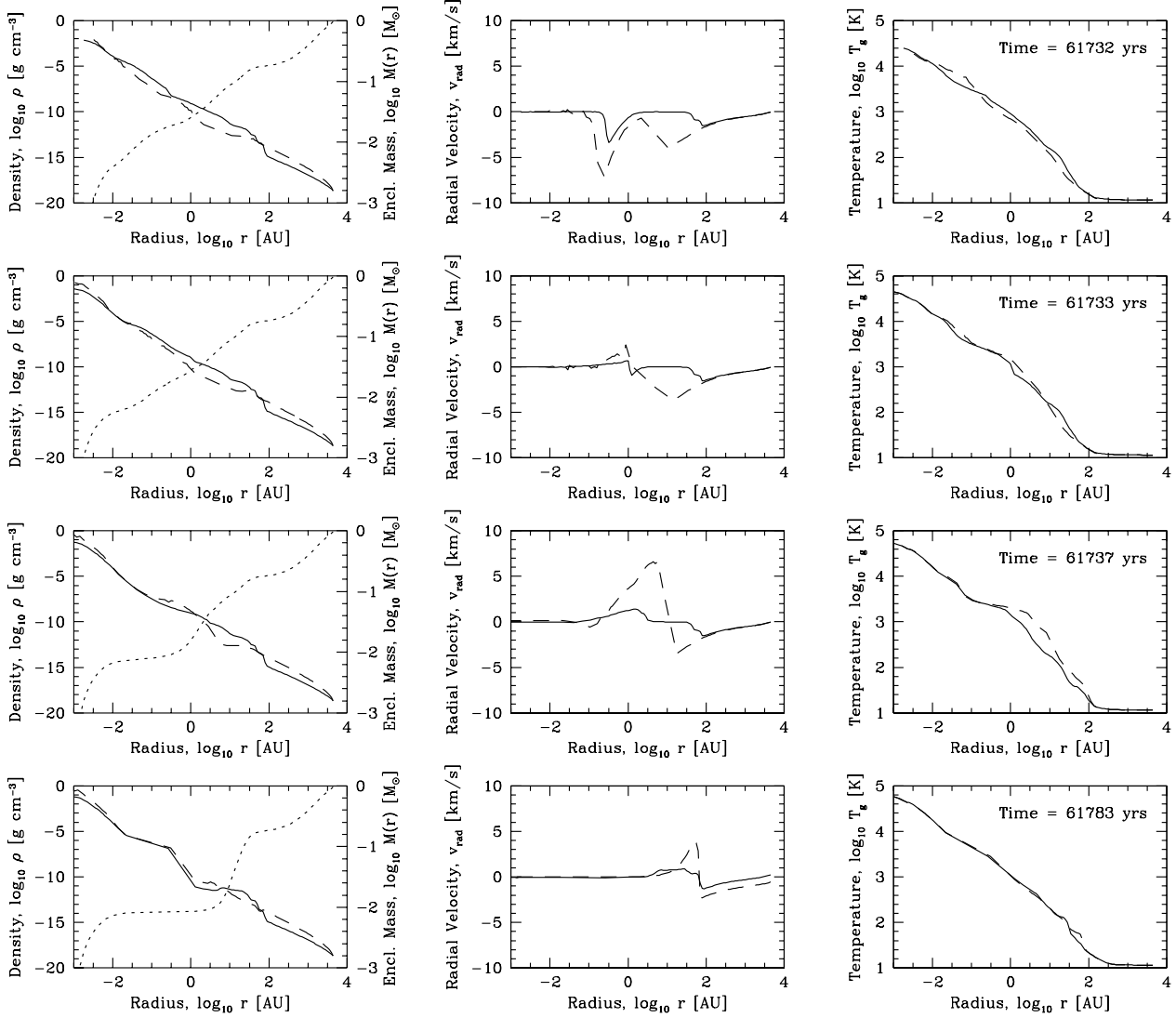


Figure 13. The evolution of the radiation hydrodynamical $\beta = 0.005$ calculation of the collapse of a molecular cloud core following stellar core formation. Each of the four rows shows the state of the protostar at different time. The left panels provide the radial density profile perpendicular to the rotation axis (solid line, averaged in azimuth), the density profile along the rotation axis (dashed line), and the cumulative mass profile (dotted line). The centre panels give the radial velocity profiles perpendicular to (solid line) or along (dashed line) the rotation axis. The right panels show the radial temperature profiles perpendicular to (solid line) or along (dashed line) the rotation axis.

the ‘holes’ around the stellar cores are in fact holes (devoid of SPH particles). However, in the high resolution $\beta = 0.001$ and $\beta = 0.005$ cases (which each use 3×10^6 particles), it is found that a small amount of gas does remain within the holes, and this gas continues to slowly accrete onto the stellar core.

In Fig. 14, we plot the mass with density $> 10^{-4} \text{ g cm}^{-3}$ versus time for the $\beta = 0.001$ and $\beta = 0.005$ cases with different resolutions. It can be seen that the mass of the stellar core at which the feedback dramatically curtails the accretion decreases from $\approx 10 - 11$ down to $6 M_{\text{J}}$ with increased resolution. For a few years, the stellar cores grow at a rate of $\sim 10^{-3} M_{\odot} \text{ yr}^{-1}$ (even with the highest resolutions). With low-resolution ($\leq 1 \times 10^6$ SPH particles), the accretion onto the stellar cores ceases entirely after the launching of the outflows due to the formation of the ‘holes’ in the inner few AU of the discs. However, using 3×10^6 SPH particles, it is found that the stellar cores do continue to accrete during this time, but at much reduced accretion rates of $2 \times 10^{-5} M_{\odot} \text{ yr}^{-1}$ for the $\beta = 0.001$ calculation and $1 \times 10^{-5} M_{\odot} \text{ yr}^{-1}$ for the

$\beta = 0.005$ calculation (measured between 20 and 50 years after stellar core formation; Fig. 14).

Although the rate of convergence with increasing resolution is relatively slow, strong outflows are launched in all cases (see Appendix A). The slow convergence is due to the strong interplay between the energy released by the formation of the stellar core, and the launching of the outflow which decreases accretion and, thus, reduces the energy that is released. If the resolution is poor, the stellar core accretes more material before the energy released feeds back and manages to stop the accretion, whereas with higher resolution, the accretion of a small amount of mass can feed thermal energy into the infalling material more quickly and, thus, inhibit further accretion.

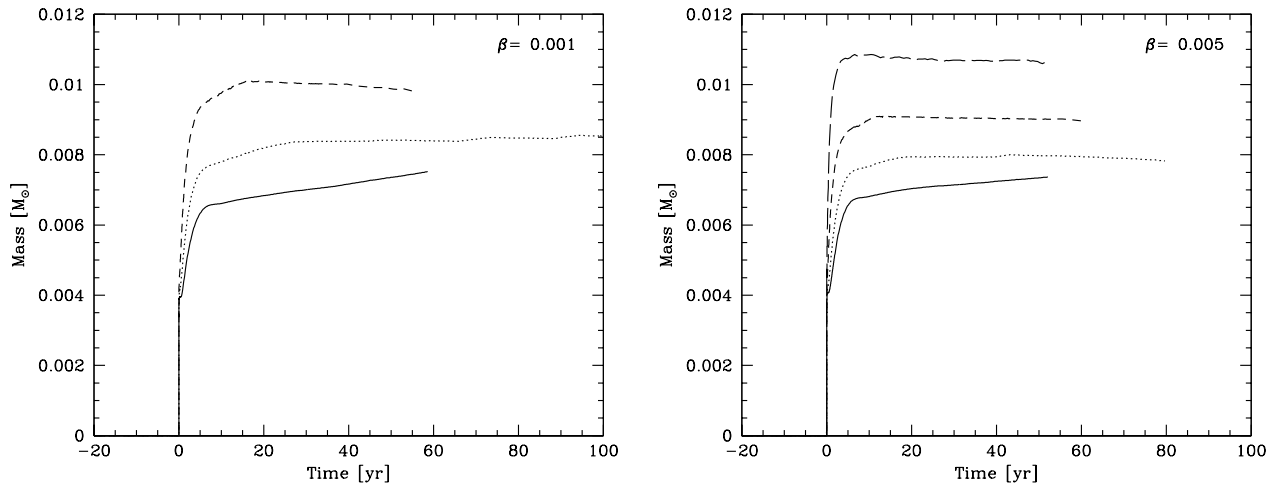


Figure 14. The mass of the stellar core (gas with density $> 10^{-4} \text{ g cm}^{-3}$) measured from the time of its formation. The two panels shows the results for the radiation hydrodynamical $\beta = 0.001$ (left) and $\beta = 0.005$ (right) molecular cloud cores performed using 10^5 (long-dashed line), 3×10^5 (short-dashed line), 10^6 (dotted line), and 3×10^6 (solid line) particles. With low resolutions the radiative feedback stops accretion onto the stellar cores, but for the highest resolutions the accretion continues at a low level ($1 - 2 \times 10^{-5} M_{\odot} \text{ yr}^{-1}$).

4 DISCUSSION

4.1 The lifetime of the first core/pre-stellar disc phase

As mentioned in Section 3.2, the introduction of radiative transfer and a realistic equation of state increases the lifetimes of the first core phase compared to that obtained using our barotropic equation of state by factors of 1.5–3 (Fig. 5). This is important, because the longer the first core phase lasts, the more easy it will be to observe. The lifetimes obtained using radiative transfer range from ≈ 400 years (with no rotation) to ≈ 3000 years (for $\beta = 0.01$), whereas using the barotropic equation of state they ranged from ≈ 100 to ≈ 1500 years. As discussed above, the difference is due to the higher temperatures (and thus higher pressures) that are obtained using the realistic physics rather than the barotropic equation of state, which slows the evolution towards the second collapse phase. This lengthening of the lifetimes with radiation hydrodynamics compared to barotropic calculations was also seen by Tomida et al. (2010). The lengthening occurs for both the non-rotating first cores, and in the cores that undergo non-axisymmetric instabilities. In the latter, once the first cores or pre-stellar discs develop the bar instability they very quickly evolve to high central densities and temperatures and undergo collapse to stellar densities when computed using the barotropic equation of state (Fig. 5, 4th and 5th panels across where the maximum density increases rapidly from 10^{-11} to $10^{-7} \text{ g cm}^{-3}$, and the maximum temperature from 100 to 2000 K). Using the more realistic physics, this evolution takes 3–8 times longer. This is because the hotter temperatures weaken the strength of the spiral arms generated by the instability (c.f. the third rows of Figs. 2 and 3) and, thus, decrease the rate of angular momentum transport within the pre-stellar disc. The removal of the angular momentum from the central regions of the disc removes rotational support from the gas (Bate 1998), allowing it to contract and heat up much more rapidly than it would due to accretion alone, eventually triggering second collapse.

The pre-stellar disc phase will be more easily observed in more rapidly-rotating molecular cloud cores because the lifetime of the phase is longer. Resolved observations of the pre-stellar disc phase (e.g. using ALMA) would also be easier and more interesting for the more rapidly-rotating cases because the disc will be much

larger (up to $\approx 50 - 100$ AU in radius rather than $\approx 5 - 10$ AU for rotationally-stable first cores) and substructure may be visible (i.e. the presence of spiral density waves). Recently, Saigo & Tomisaka (2011) investigated the observability of pre-stellar discs using ALMA and concluded that ALMA should be able to image objects in the nearest star-forming regions. For the particular initial conditions used in this paper, the lifetimes of as a function of the initial cloud rotation rate are plotted in Fig. 15. As pointed out recently by Tomida et al. (2010), the lifetime of the first core phase also depends on the mass of the molecular cloud core such that the lifetimes are longer in lower-mass molecular cloud cores. For initial core masses of $\approx 0.1 M_{\odot}$, the accretion onto the first core/pre-stellar disc is not sufficient to drive the object into the second collapse phase. Instead, the central regions of the first core/disc evolve to higher temperatures primarily through radiative cooling. As the first core radiates energy, it contracts and heats up, eventually exceeding 2000 K when the dissociation of molecular hydrogen begins, but this process can take in excess of 10^4 years. Thus, the first core/pre-stellar disc phase is more likely to be observed for molecular cloud cores that have higher rotation rates and lower masses.

Despite this, observing the pre-stellar disc phase with ALMA will be challenging. Lifetimes of even $4 \times 10^3 - 10^4$ years are still only 2–5% of the estimates of Class 0 lifetimes of 2×10^5 yrs (Hatchell et al. 2007; Evans et al. 2009), so that for every 100 Class 0 objects there should only be a few pre-stellar discs. The first place to look is likely to be the so-called very low luminosity objects (VeLLOs) with luminosities of less than $0.1 L_{\odot}$ (e.g. Young et al. 2004; Crapsi et al. 2005; Huard et al. 2006; Bourke et al. 2006), some of which have recently been proposed as candidate first cores (Chen et al. 2010; Enoch et al. 2010).

4.2 Disc to stellar mass ratios

As first discovered by Bate (1998), a rotating first core actually leads to a disc that forms *before* the star. These discs can range from ≈ 5 AU in radius for very slowly rotating first cores (c.f. Larson 1969) to ≈ 100 AU for cores that undergo rotational instabilities (Machida et al. 2010; Bate 2010; Machida & Matsumoto 2011).

Because the disc forms first, there is always a phase of star formation when the disc to stellar mass ratio is greater than unity. For example, in the original calculation of Bate (1998), the disc had a mass of $0.08 M_{\odot}$ when the stellar core formed with an initial mass of only $1.5 M_{\text{J}}$, giving a disc to stellar mass ratio $\gtrsim 50$. Although some quite massive discs have been discovered around some young stars (e.g. the $0.8 M_{\odot}$ disc around a $3.5 M_{\odot}$ star; Hamidouche 2010) such cases are rare (e.g. Boissier et al. 2011) and the usual assumption is that the circumstellar disc mass is always likely to be less than the stellar mass. While this is almost certainly true later in the evolution of a protostar (e.g. Class I or Class II low-mass objects and Herbig Ae/Be stars), in the very earliest phases the disc to star mass ratio can greatly exceed unity.

With the initial conditions used in this paper, the disc mass when the stellar core forms increases with the rotation rate of the progenitor molecular cloud core. This is because a greater fraction of the $1 M_{\odot}$ molecular cloud core has sufficient angular momentum to settle outside the typical 5 AU radius of a non-rotating first core. Because more mass settles away from the centre of the object, the accretion from the infalling envelope is less effective at increasing the central temperature (i.e. mass receives support from rotation as well as thermal pressure). Thus, the first core phase lasts longer and the masses of the first cores/pre-stellar discs at the time of stellar core formation range from $\approx 0.03 M_{\odot}$ for $\beta = 0$ to $\approx 0.22 M_{\odot}$ for $\beta = 0.01$ (see Fig. 15 and the dotted lines in the left panels of Figs. 12 to 13). In the most extreme case we have modelled here, when the stellar core forms with an initial mass of $\approx 2 M_{\text{J}}$, the disc is more than 100 times more massive than the star! Note that the initial rotation rate of the molecular cloud core is *not* extreme for this case. Goodman et al. (1993) find that the values of β for observed molecular cloud cores range from 0.002 to > 1 , with typical values of $\beta \sim 0.02$. Therefore, it is quite possible that when pre-stellar discs are observed (e.g. with ALMA), they could have substantial masses (e.g. up to 1/4 of the mass of an entire $1 M_{\odot}$ molecular cloud core) without a stellar core having formed.

4.3 Disc fragmentation

The potential for high disc to stellar mass ratios also implies that some of these discs may fragment very early in the star formation process. Indeed, for our $\beta = 0.01$ case (and, of course, the $\beta = 0.04$ case), this is exactly what happens, with the disc fragmenting to produce two additional ‘first cores’ even before the original first core/disc has undergone second collapse to produce a stellar core. The fate of such fragments is of course not clear. Multiple fragments may merge with each other before they each undergo second collapse. They may also spiral in to the central object and be disrupted before they undergo second collapse. However, those that survive will produce the seeds of binary or multiple stellar systems.

As pointed out by Whitehouse & Bate (2006), Krumholz (2006), Krumholz et al. (2007), Bate (2009) and Offner et al. (2009), radiative feedback from newly formed protostars heats their surrounding gas and inhibits fragmentation. In star cluster formation simulations (e.g. Bate 2009; Offner et al. 2009) this radiative heating dramatically reduces the number of objects formed compared to using a barotropic equation of state. Some of this reduction comes from a reduction in the frequency of disc fragmentation because the discs are heated and stabilised by the radiation from their central objects (Bate 2009).

However, as shown here in the $\beta = 0.01$ case, fragmentation of the pre-stellar disc resulting from a rapidly-rotating first core

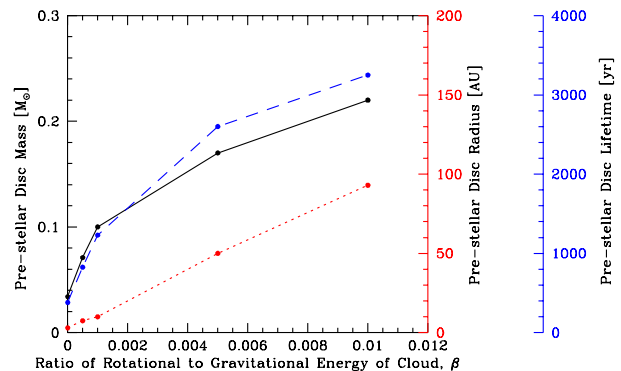


Figure 15. The dependence of the pre-stellar disc (first core) properties on the initial rotation rate of the progenitor molecular cloud core, β . We plot the masses and radii of the pre-stellar cores, measured just before the second collapse to form the stellar core occurs, and the lifetime of the pre-stellar disc (i.e. the time between the formation of a first hydrostatic core and the formation of the stellar core). The mass, radius, and lifetime all increase with larger initial molecular cloud core rotation rates. In the more rapidly-rotating cases, the pre-stellar disc accumulates a significant fraction of the total cloud mass before the stellar core forms. Note that most rapidly-rotating $\beta = 0.04$ case has been excluded because it forms four fragments rather than a single pre-stellar disc.

phase can occur *before* the central stellar core is formed. Thus, even if radiative feedback can completely stop disc fragmentation after the stellar core forms, disc fragmentation *before* stellar core formation may be a common route to forming binary and multiple systems.

4.4 Implications of radiative feedback following stellar core formation

The radiative impact of stellar core formation on the surrounding disc, driving a shock wave through the disc and launching an outflow may have several wider implications. These were discussed by Bate (2010), so we only briefly list them here. First, in future studies it will be important to examine the relative roles of radiative heating due to stellar core formation and magnetic fields in the launching of a protostellar jet. Second, although the outburst and the dramatic decrease in the stellar core accretion rate discussed in this paper is a transient associated with stellar core formation, it might reoccur if the accretion rate onto the stellar core increases again and, thus, may potentially be a source of episodic accretion and outbursts. Third, such outbursts may contribute to the production of the chondrules found in meteorites (Grossman et al. 1988).

5 CONCLUSIONS

We have presented results from three-dimensional radiation hydrodynamical calculations that follow the collapse of a molecular cloud core through the formation and evolution of the first hydrostatic core and beyond the formation of the stellar core. We find the evolution before the formation of the stellar core is qualitatively similar to that found in the past using barotropic equations of state. As found in past studies, the evolution of the first hydrostatic core depends on the initial rotation rate of the cloud. Non-rotating

or slowly rotating clouds produce small spherical or weakly flattened first cores with radii of $\approx 5 - 10$ AU. More rapidly rotating clouds ($\beta \approx 0.001 - 0.01$) produce highly-oblate rapidly-rotating first cores that undergo dynamic rotational instabilities to produce large discs (radii $\approx 10 - 100$ AU) before the formation of a stellar core. These objects are better described as pre-stellar discs than first cores. Yet more rotation typically results in fragmentation, via a torus shaped first core if the initial cloud is axisymmetric. Quantitatively, using radiation hydrodynamics with a realistic equation of state produces first cores that are somewhat hotter, slightly more stable to rotational instabilities, and longer-lived (by factors of 1.5 – 3) than using our barotropic equation of state.

The masses and radii of the pre-stellar discs produced before stellar core increase with the initial rotation rate of the molecular cloud core. Their lifetimes also increase with rotation rate, and for lower-mass molecular cloud cores (see also Tomida et al. 2010). With high rotation rates, these pre-stellar discs can have radii up to ≈ 100 AU and contain in excess of $0.2 M_{\odot}$ of gas (up to $1/4$ of the mass of the entire molecular cloud core) and exist for several thousands of years before stellar core formation. Such objects may be resolvable by ALMA. Since initial mass of the stellar core which forms within these discs is just a few Jupiter-masses, the disc-to-star mass ratios can exceed 100 for a short period of time.

Fragmentation of a pre-stellar disc prior to stellar core formation may be an effective way to produce binary and multiple star systems because the radiative feedback from the stellar core which may inhibit later fragmentation of a massive disc is absent.

After the formation of a stellar core within the disc, dissociating gas from the inner regions of the disc falls towards the stellar core and builds a smaller disc around the stellar core. This inner disc increases with radius as material with higher angular momentum falls in, and eventually merges with the inner edge of the outer disc.

Although this inner/outer disc structure and the earlier evolution of the first core phase is similar for barotropic and radiation hydrodynamical calculations, we find that the subsequent evolution is qualitatively different in radiation hydrodynamical calculations. In barotropic calculations, the formation of the stellar core deep inside the first core (or pre-stellar disc) has no effect on the surrounding disc because the temperature of the gas is simply set by the density of the gas. However, with radiation hydrodynamics, the energy released by the formation of the stellar core within the optically thick disc is similar to the binding energy of the disc. This heats region surrounding the stellar core and, at approximately the same time as the inner disc and outer discs merge, a shock wave forms in the merger region and propagates outwards through the disc, while a bipolar outflow is launched perpendicular to the rotation axis, dramatically decreasing the accretion rate on to the stellar core. The properties of the outflow do not seem to vary greatly with the initial rotation rate of the molecular cloud core or the pre-stellar disc, but the speed of the outflow is somewhat greater for higher rotation rates and the shockwave which propagates outward through the disc reaches the outer edge of the disc more quickly for smaller discs. It remains to be seen how the inclusion of magnetic fields alters this thermally-driven outburst.

ACKNOWLEDGMENTS

MRB is grateful for the hospitality and support he received from the Monash Centre for Astrophysics while on study leave and where

this paper was written up. The calculations for this paper were performed on the University of Exeter Supercomputer, a DiRAC Facility jointly funded by STFC, the Large Facilities Capital Fund of BIS, and the University of Exeter. Some figures were produced using the publicly available SPLASH visualisation software (Price 2007). This work, conducted as part of the award “The formation of stars and planets: Radiation hydrodynamical and magnetohydrodynamical simulations” made under the European Heads of Research Councils and European Science Foundation EURYI (European Young Investigator) Awards scheme, was supported by funds from the Participating Organisations of EURYI and the EC Sixth Framework Programme.

REFERENCES

- Alexander D. R., 1975, *ApJS*, 29, 363
 Bate M. R., 1998, *ApJ*, 508, L95
 Bate M. R., 2009, *MNRAS*, 392, 1363
 Bate M. R., 2010, *MNRAS*, 404, L79
 Bate M. R., Bonnell I. A., Price N. M., 1995, *MNRAS*, 277, 362
 Bate M. R., Burkert A., 1997, *MNRAS*, 288, 1060
 Benz W., 1990, in Buchler J. R., ed., *Numerical Modelling of Nonlinear Stellar Pulsations Problems and Prospects*. Kluwer, Dordrecht, p. 269
 Benz W., Cameron A. G. W., Press W. H., Bowers R. L., 1990, *ApJ*, 348, 647
 Boissier J., Alonso-Albi T., Fuente A., Berne O., Bachiller R., Neri R., Ginard D., 2011, *ArXiv e-prints*
 Boley A. C., Hartquist T. W., Durisen R. H., Michael S., 2007, *ApJ*, 656, L89
 Boss A. P., Fisher R. T., Klein R. I., McKee C. F., 2000, *ApJ*, 528, 325
 Bourke T. L., Myers P. C., Evans II N. J., Dunham M. M., Kauffmann J., Shirley Y. L., Crapsi A., Young C. H., Huard T. L., Brooke T. Y., Chapman N., Cieza L., Lee C. W., Teuben P., Wahhaj Z., 2006, *ApJ*, 649, L37
 Cha S., Whitworth A. P., 2003, *MNRAS*, 340, 91
 Chen X., Arce H. G., Zhang Q., Bourke T. L., Launhardt R., Schmalzl M., Henning T., 2010, *ApJ*, 715, 1344
 Commerçon B., Audit E., Chabrier G., Chièze J.-P., 2011, *A&A*, 530, A13+
 Crapsi A., Devries C. H., Huard T. L., Lee J.-E., Myers P. C., Ridge N. A., Bourke T. L., Evans II N. J., Jørgensen J. K., Kauffmann J., Lee C. W., Shirley Y. L., Young C. H., 2005, *A&A*, 439, 1023
 Durisen R. H., Gingold R. A., Tohline J. E., Boss A. P., 1986, *ApJ*, 305, 281
 Enoch M. L., Lee J.-E., Harvey P., Dunham M. M., Schnee S., 2010, *ApJ*, 722, L33
 Evans II N. J., Dunham M. M., Jørgensen J. K., Enoch M. L., Merín B., van Dishoeck E. F., Alcalá J. M., Myers P. C., Stapelfeldt K. R., Huard T. L., Allen L. E., Harvey P. M., van Kempen T., et al. 2009, *ApJS*, 181, 321
 Goodman A. A., Benson P. J., Fuller G. A., Myers P. C., 1993, *ApJ*, 406, 528
 Grossman J. N., Rubin A. E., Nagahara H., King E. A., 1988, in Kerridge J. F., Matthews M. S., eds, *Meteorites and the Early Solar System*. Univ. of Arizona Press, Tucson, p. 619
 Hamidouche M., 2010, *ApJ*, 722, 204
 Hatchell J., Fuller G. A., Richer J. S., Harries T. J., Ladd E. F., 2007, *A&A*, 468, 1009

- Huard T. L., Myers P. C., Murphy D. C., Crews L. J., Lada C. J., Bourke T. L., Crapsi A., Evans II N. J., McCarthy Jr. D. W., Kulesa C., 2006, *ApJ*, 640, 391
- Krumholz M. R., 2006, *ApJ*, 641, L45
- Krumholz M. R., Klein R. I., McKee C. F., 2007, *ApJ*, 656, 959
- Larson R. B., 1969, *MNRAS*, 145, 271
- Larson R. B., 1972, *MNRAS*, 156, 437
- Machida M. N., Inutsuka S., Matsumoto T., 2006, *ApJ*, 647, L151
- Machida M. N., Inutsuka S., Matsumoto T., 2010, *ArXiv e-prints*
- Machida M. N., Inutsuka S.-i., Matsumoto T., 2007, *ApJ*, 670, 1198
- Machida M. N., Inutsuka S.-i., Matsumoto T., 2008, *ApJ*, 676, 1088
- Machida M. N., Matsumoto T., 2011, *MNRAS*, pp 284+
- Machida M. N., Matsumoto T., Hanawa T., Tomisaka K., 2005, *MNRAS*, 362, 382
- Masunaga H., Inutsuka S.-I., 2000, *ApJ*, 531, 350
- Morris J. P., Monaghan J. J., 1997, *J. Comp. Phys.*, 136, 41
- Norman M. L., Wilson J. R., 1978, *ApJ*, 224, 497
- Offner S. S. R., Klein R. I., McKee C. F., Krumholz M. R., 2009, *ApJ*, 703, 131
- Pollack J. B., McKay C. P., Christofferson B. M., 1985, *Icarus*, 64, 471
- Price D. J., 2007, *Publ. Astron. Soc. Australia*, 24, 159
- Price D. J., Bate M. R., 2007, *MNRAS*, 377, 77
- Price D. J., Monaghan J. J., 2005, *MNRAS*, 364, 384
- Price D. J., Monaghan J. J., 2007, *MNRAS*, 374, 1347
- Saigo K., Tomisaka K., 2006, *ApJ*, 645, 381
- Saigo K., Tomisaka K., 2011, *ApJ*, 728, 78
- Saigo K., Tomisaka K., Matsumoto T., 2008, *ApJ*, 674, 997
- Schönke J., Tschamuter W. M., 2011, *A&A*, 526, A139+
- Stamatellos D., Whitworth A. P., Bisbas T., Goodwin S., 2007, *A&A*, 475, 37
- Tomida K., Machida M. N., Saigo K., Tomisaka K., Matsumoto T., 2010, *ApJ*, 725, L239
- Tomida K., Tomisaka K., Matsumoto T., Ohsuga K., Machida M. N., Saigo K., 2010, *ArXiv e-prints*
- Tomisaka K., 2002, *ApJ*, 575, 306
- Tschamuter W. M., 1987, *A&A*, 188, 55
- Tschamuter W. M., Schönke J., Gail H., Tieloff M., Lüttjohann E., 2009, *A&A*, 504, 109
- Whitehouse S. C., Bate M. R., 2006, *MNRAS*, 367, 32
- Whitehouse S. C., Bate M. R., Monaghan J. J., 2005, *MNRAS*, 364, 1367
- Young C. H., et al. 2004, *ApJS*, 154, 396

APPENDIX A: NUMERICAL CONVERGENCE OF THE RADIATION HYDRODYNAMICAL CALCULATIONS

As mentioned in Section 2.2, for the different initial conditions and equations of state discussed in this paper, most of the calculations were performed with several different numerical resolutions to check for numerical convergence of the results. The numbers of SPH particles used were 1×10^5 , 3×10^5 , 1×10^6 , and 3×10^6 particles, although as summarised in Table 1 not all cases were performed with all resolutions. The only type of calculation to be performed with all four resolutions was the $\beta = 0.005$ case with radiation hydrodynamics, but the evolution of three other initial conditions performed with radiation hydrodynamics were studied with two ($\beta = 0.01$ and 0.04) or three ($\beta = 0.001$) different resolutions.

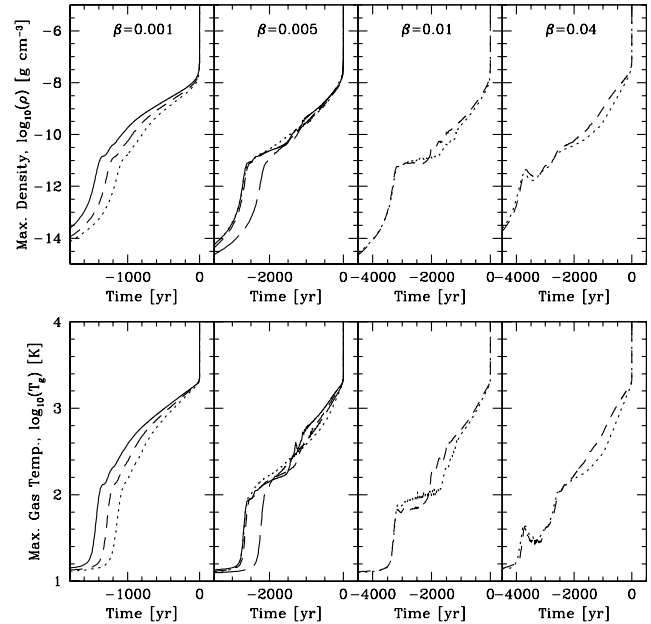


Figure 16. Examining the numerical convergence of the lifetime and evolution of the first core/disc. We plot the time evolution of the maximum density (upper panels) and gas temperature (lower panels) during the radiation hydrodynamical calculations of the collapse of molecular cloud cores with different initial rotation rates. From left to right, the different panels are for cloud cores with $\beta = 0.001, 0.005, 0.01, 0.04$. The different line types are for calculations performed using 1×10^5 (long-dashed line), 3×10^5 (dotted lines), 1×10^6 (short-dashed lines), and 3×10^6 (solid lines) SPH particles. Time is set to zero at the end of the second dynamic collapse phase when the density reaches $10^{-3} \text{ g cm}^{-3}$ which allows the length of the first hydrostatic core phases to be compared. It can be seen that the lifetime of the first core phase is well converged for all except the lowest resolution calculation for the $\beta = 0.005$ case, and the $\beta = 0.001$ case. This is because the lifetime of the first core/disc is determined by the dynamic rotational instability for $\beta \geq 0.005$, whereas for $\beta = 0.001$ viscous evolution probably plays a significant role.

In this appendix, we discuss how the results depend on numerical resolution.

As numerical resolution was increased, all of the clouds took slightly longer to collapse. However, more important for the results presented in the main sections of this paper is how the lifetime and evolution of the first core or pre-stellar disc phase depends on numerical resolution. In Figure 16, we plot the evolution of maximum density and temperature versus the time before stellar core formation (defined as when the maximum density reaches $10^{-3} \text{ g cm}^{-3}$) for the radiation hydrodynamical calculations with $\beta = 0.001 - 0.04$. The lifetimes of the pre-stellar disc phase are all well converged for $\geq 3 \times 10^5$ particles, with the exception of the $\beta = 0.001$ case. For the $\beta = 0.005 - 0.04$ cases, the lifetime of the first core/pre-stellar disc phase depends on the development of dynamical non-axisymmetric instabilities due to the high ratio of the rotational to gravitational potential energies. In particular, the transport of angular momentum via gravitational torques from the spiral density waves removes rotational support from the gas and drives the object to the second collapse phase much more quickly than it would evolve due to accretion and radiative cooling alone (see Section 3.2). However, the $\beta = 0.001$ case is rotationally stable. Therefore, it evolves to the second collapse phase through accretion and radiative cooling, but also through angular momentum

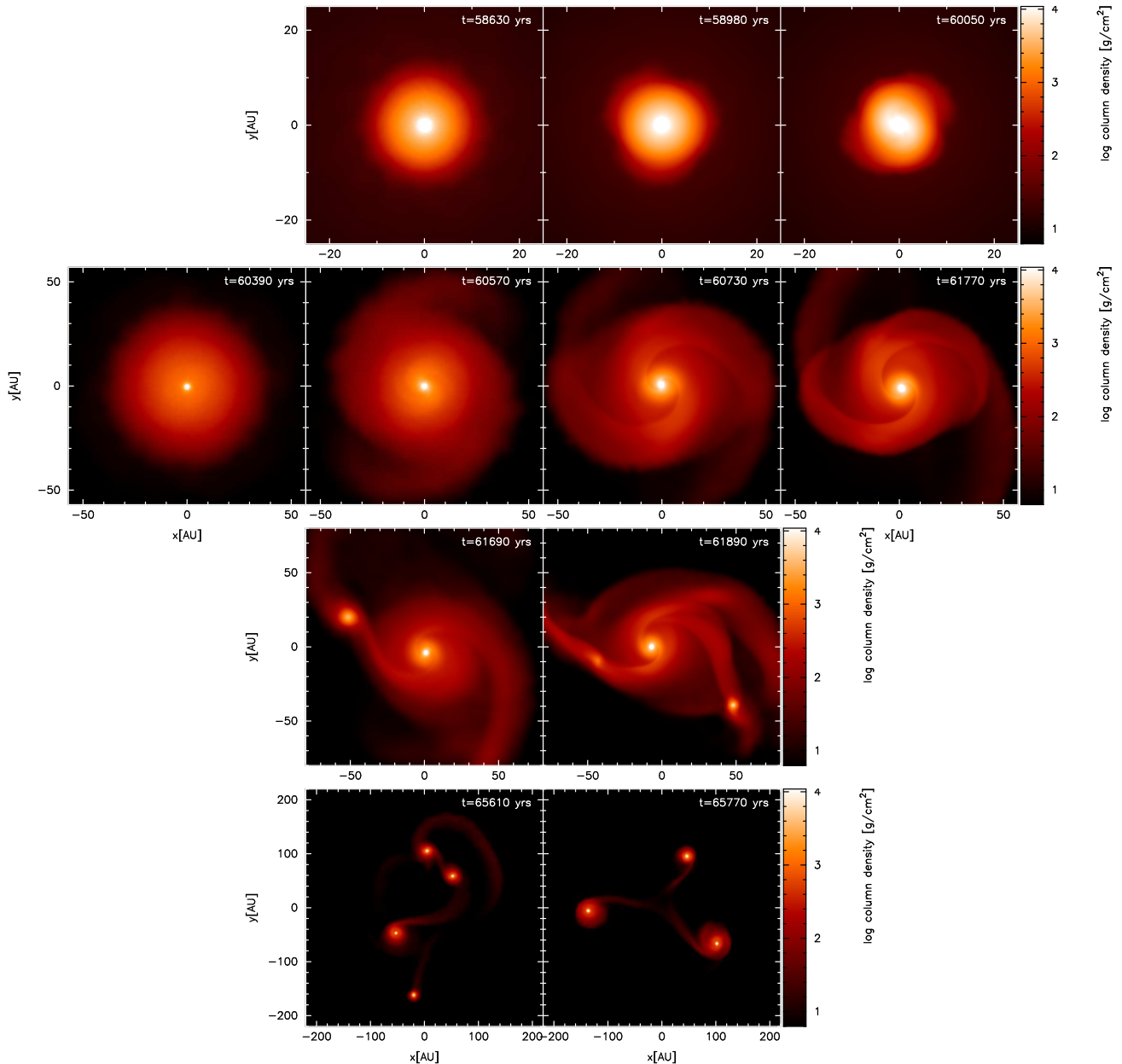


Figure 17. Snapshots of the column density viewed along the rotation axis at the point of stellar core formation (defined as when the maximum density reaches $1 \times 10^{-3} \text{ g cm}^{-3}$). From top to bottom, the different rows are for molecular cloud cores with $\beta = 0.001, 0.005, 0.01, 0.04$. Note that the spatial scale is different for each row. From left-to-right, the columns are for calculations performed with $1 \times 10^5, 3 \times 10^5, 1 \times 10^6$, and 3×10^6 SPH particles. For each rotation rate, the evolution is qualitatively the same when using 3×10^5 particles or more.

transport by numerical shear viscosity. Numerical shear viscosity will transport angular momentum outwards, reducing the rotational support of the gas in the centre of the first core, driving it more quickly to higher densities and temperatures and, thus, hastening the onset of the second collapse. As the resolution is increased, the numerical shear viscosity decreases. Therefore, it is most likely that the longer lifetimes of the pre-stellar disc phase for the $\beta = 0.001$ case with increasing resolution is due to the effect of the numerical shear viscosity in SPH. We also note that the dominant term in the numerical viscosity (the α_v term) is first-order, which explains why the convergence with increasing resolution is quite slow (left panels of Figure 16). Thus, for the first cores which do not undergo

dynamical rotational instabilities, the lifetimes obtained in this paper should be treated as lower limits.

In Fig. 17, we plot images of the first cores/pre-stellar discs at the time of stellar core formation for the $\beta = 0.001 - 0.04$ radiation hydrodynamical cases obtained using the different numerical resolutions. For the $\beta = 0.001$ case, the first core is right at the boundary of rotational stability, with a very weak spiral instability visible in the highest resolution case. For the $\beta = 0.005$ case, all resolutions except the lowest (1×10^5 particles) resolve the rotational instability. As the resolution is increased, the sharpness of the spiral density waves improves and the pre-stellar disc becomes slightly smaller, but the structure definitely seems to be converging. For the $\beta = 0.01$ case, there are only two resolutions. Both pro-

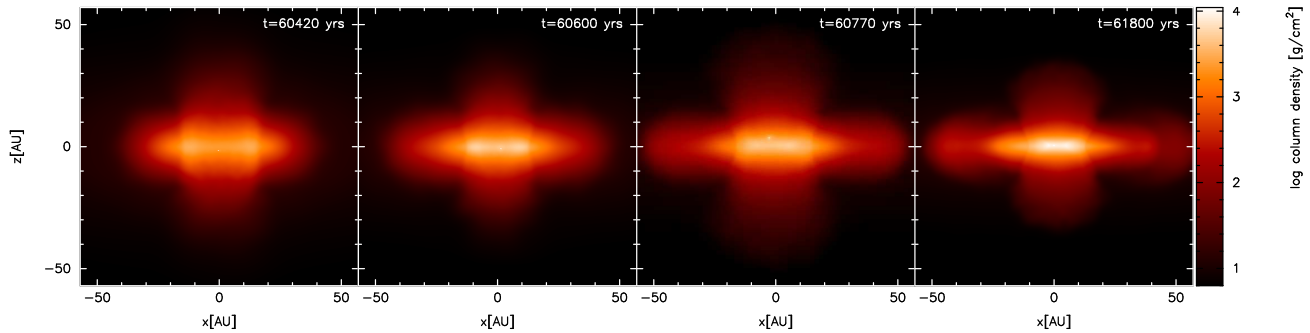


Figure 18. Snapshots of the column density viewed perpendicular to the rotation axis 25 years after stellar core formation (defined as when the maximum density reaches $1 \times 10^{-3} \text{ g cm}^{-3}$) in a $\beta = 0.005$ molecular cloud core. From left to right, the different panels are for radiation hydrodynamical calculations performed with 1×10^5 , 3×10^5 , 1×10^6 , and 3×10^6 SPH particles. The bipolar outflow and the shockwave propagating through the disc are similar in all cases, regardless of the resolution.

duce a central object surrounded by a disc of radius ≈ 90 AU which fragments. The higher resolution case forms two fragments, while the lower resolution case only has one fragment. Thus, while the number of fragments has not converged, the size of the pre-stellar disc and the fact that it does fragment seem to be robust. Finally, both resolutions of the $\beta = 0.04$ case produce ring-type first cores which fragment into four separate cores. However, with four objects the subsequent evolution becomes chaotic. In the 3×10^5 particle calculation, the four fragments survive (at least until the first undergoes second collapse), but in the 1×10^6 particle calculation two of the objects merge producing a triple system (see the bottom rows of Fig. 17 and 3).

Following stellar core formation, as discussed in detail in Section 3.3, a bipolar outflow is launched perpendicular to the disc and a shockwave propagates outwards along the plane of the disc. These outflows and shockwaves occur in all of the radiation hydrodynamical simulations, with the exception of the spherically-symmetric $\beta = 0$ case. This result does not appear to depend on resolution (see Figure 18). However, as discussed in Section 3.3 and illustrated in Fig. 14, the initial mass of the stellar core and its accretion rate are affected by resolution.

In summary, we conclude that the lifetimes of the first cores/pre-stellar discs are well converged for initial conditions that produce rotationally-unstable pre-stellar discs, but that for more slowly-rotating cores (i.e. $\beta = 0.0005$ and $\beta = 0.001$) the lifetimes are lower-limits. We also find that the qualitative outcomes (rotationally-stable first core, pre-stellar disc with spiral arms, fragmenting pre-stellar disc, and torus) are numerically-converged but the details (e.g. how many fragments) may not be.